MASARYKOVA UNIVERZITA
PŘÍRODOVĚDECKÁ FAKULTA
ÚSTAV TEORETICKÉ FYZIKY A ASTROFYZIKY

Diplomová práce

BRNO 2017 **MARTIN PIECKA**

MASARYKOVA UNIVERZITA
PŘÍRODOVĚDECKÁ FAKULTA
ÚSTAV TEORETICKÉ FYZIKY A ASTROFYZIKY

Tracing a Possible Carrier of Diffuse Interstellar Bands

Diplomová práce

Martin Piecka

Vedoucí práce: doc. Mgr. Ernst Paunzen, Dr. **Brno 2017**

Bibliografický záznam

Autor:	Martin Piecka Přírodovědecká fakulta, Masarykova univerzita Ústav teoretické fyziky a astrofyziky
Název práce:	Tracing a Possible Carrier of Diffuse Interstellar Bands
Studijní program:	Fyzika
Studijní obor:	Astrofyzika
Vedoucí práce:	doc. Mgr. Ernst Paunzen, Dr.
Akademický rok:	2016/2017
Počet stran:	$8 + 51$
Klíčová slova:	Mezihvězdné prostředí; difúzní mezihvězdná pásma; spektrální čáry; zdroje čar; Morseův potenciál; buckminsterfullerene

Bibliographic Entry

Author:	Martin Piecka Faculty of Science, Masaryk University Department of Theoretical Physics and Astrophysics
Title of Thesis:	Tracing a Possible Carrier of Diffuse Interstellar Bands
Degree Programme:	Physics
Field of Study:	Astrophysics
Supervisor:	doc. Mgr. Ernst Paunzen, Dr.
Academic Year:	2016/2017
Number of Pages:	$8 + 51$
Keywords:	Interstellar medium; Diffuse interstellar bands; Spectral lines; Carriers of the lines; Morse potential; Buckminsterfullerene

Abstrakt

V této diplomové práci se snažíme vytvořit rovibrační model fullerénu C_{60}. Cílem je navázat na laboratorní přiřazení dvou difúzních mezihvězdných pásem k této molekule.

V teoretické části práce se zabýváme difúzními mezihvězdnými pásmy, zkoumáme fáze mezihvězného prostředí a analyzujeme použitelné rotační a vibrační modely molekul. Praktická část je zaměřena na vytváření modelu fullerénu a testování získaných výsledků.

Abstract

In this thesis, we attempt to create a rovibrational model of the buckminsterfullerene, C_{60}. The aim is to address the laboratory assignment of two diffuse interstellar bands to this molecule.

In the theoretical part of the thesis, we deal with the diffuse interstellar bands, investigate different phases of the interstellar medium and analyse applicable rotational and vibrational models of molecules. The practical part is focused on the derivation of the model of the buckminsterfullerene and testing the calculated results.

MASARYKOVA UNIVERZITA
Přírodovědecká fakulta

ZADÁNÍ DIPLOMOVÉ PRÁCE

Akademický rok: 2016/2017

Ústav: Ústav teoretické fyziky a astrofyziky

Student: Bc. Martin Piecka

Program: Fyzika

Obor: Teoretická fyzika a astrofyzika

Směr: Astrofyzika

Ředitel *Ústavu teoretické fyziky a astrofyziky* PřF MU Vám ve smyslu Studijního a zkušebního řádu MU určuje diplomovou práci s názvem:

Název práce: Tracing a possible carrier of Diffuse Interstellar Bands

Název práce anglicky: Tracing a possible carrier of Diffuse Interstellar Bands

Oficiální zadání:
The diffuse interstellar bands (DIBs) are absorption lines seen towards reddened stars. None of the molecules responsible for these bands have been conclusively identified, yet. Recently, Campbell et al. (2015, Nature, 523, 322) reported that the C60+ molecule is a good candidate for two lines in the red optical spectrum. Within this thesis, the results of Campbell et al. should be recalculated and further possible DIBs should be identified. On the basis of the derived model also other C molecules might be investigated as possible carriers.

Literatura:
SPITZER, Lyman. *Fizičeskije processy v mežzvezdnoj srede : Physical processes in the interstellar medium*. Moskva: Mir, 1981. 349 s.

Jazyk závěrečné práce: angličtina

Vedoucí práce: doc. Mgr. Ernst Paunzen, Dr.

Datum zadání práce: 23. 2. 2016

V Brně dne: 27. 2. 2017

Souhlasím se zadáním (podpis, datum):

Piecka
.....
Bc. Martin Piecka
student

.....
doc. Mgr. Ernst Paunzen, Dr.
vedoucí práce

.....
prof. Rikard von Unge, Ph.D.
ředitel Ústavu teoretické fyziky a astrofyziky

Acknowledgement

I would like to thank my supervisor doc. Mgr. Ernst Paunzen, Dr. for his advice and much needed support during the process of the research and completion of this thesis.

Prohlášení

Prohlašuji, že jsem svoji diplomovou práci vypracoval samostatně s využitím informačních zdrojů, které jsou v práci citovány.

Brno 2017 .....

Martin Piecka

Contents

Introduction

Over the past three thousand years, a great progress has been made towards the understanding of the universe. While in the past we thought that stars are immobile bodies positioned on a sphere around the Earth, we know today that they are in fact distant giant plasmatic spheroids which orbit centres of their host galaxies. There is, however, no void between these objects – the vast space between stars and galaxies is filled with matter which is arguably just us important for understanding of the universe as are the stars themselves. Most studied is the gaseous form of the matter. The disadvantage of studying this so-called interstellar (or intergalactic) medium is that we usually cannot observe it directly and we have to rely on its effects on the light coming from the stars behind the medium.

In stellar astrophysics, it is very important to know the composition of the interstellar medium from which the stars are born. When modelling stellar atmospheres, one can stick with simple approximations, but knowledge of the present atoms and molecules helps us to create better models. On the other hand, the composition of the interstellar clouds is known to determine the evolution of astrophysical bodies. Although it seems that most of atoms and molecules important in the interstellar medium have already been discovered, there still remain many unknown absorption features that can be observed in spectra of distant objects. Many of these features are located in near ultraviolet, visible and near-infrared parts of the spectrum and are usually referred to as diffuse interstellar bands. Carriers of these features are still unknown but recently, in 2015, a laboratory experiment showed that one of the fullerenes – buckminsterfullerene C_{60} – could be responsible for at least two of these bands.

The theoretical determination of the carrier of absorption features is usually very hard, if not impossible, especially in the case of large molecules. It requires either laboratory measurements or a precise calculation of energy levels which may not be as straightforward as it is in the case of diatomic molecules. However, properties and the symmetry of buckminsterfullerene may help to solve this problem and any model created can be checked by looking in the spectra of stars.

Chapter 1

Diffuse Interstellar Bands

Diffuse interstellar bands (DIBs) are spectral absorption features found in the lines of sight of astrophysical objects, especially reddened hot stars. They are believed to originate from the interstellar medium. This has been proved by observing binary systems of stars whose spectral lines are shifted due to the Doppler effect, but no significant difference between wavelengths of DIBs has been detected. Another proof of their interstellar origin can be found by plotting their equivalent widths against Galactic coordinates (Galactic latitude b or the coordinate z perpendicular to the Galactic disc).

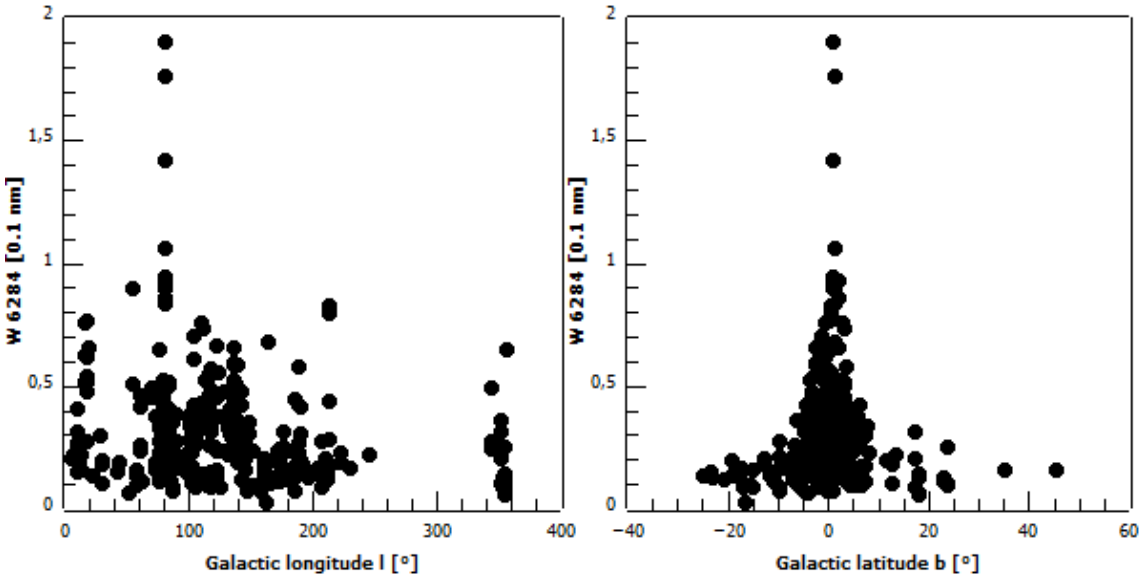

Figure 1.1: Correlations between the equivalent width of the DIB at 6284 Å, Galactic longitude l (left) and latitude b (right), based on the data from Snow et al. (1977).

Although there are hundreds of articles concerning DIBs, it is difficult to find information about individual features, since there does not appear to be any correlation between the bands themselves but there are some exceptions detected. Therefore, in order to investigate DIBs, one has to study their common properties and only with very-high-resolution spectroscopy, subtle features of a DIB can be detected.

1.1 Several Strong Bands

To this date, hundreds of DIBs have already been identified. Since most of them are very narrow and weak, there are only several DIBs which have been intensively studied. These have the property of being quite strong and appear in the most of the spectra of reddened stars. We will shortly discuss what we know about some of them and how they are related to other DIBs and other absorption features.

1.1.1 5780 Å and 5797 Å DIBs

Discovered in the early 1920s (Heger, 1922), 5780 **Å** and 5797 **Å** were the first detected DIBs. It took more than a decade for astronomers to realise that the investigation of these unknown features is important.

Since then, these bands were extensively studied. The work done by Krełowski et al. (1993) would be used as an example. They observed spectra of 8 stars of spectral classes O and B with $E(B-V) > 0.3$ mag. The research team found that two other DIBs are somehow related to 5780 Å and 5797 Å DIBs. Absorption feature at 5844 Å appears to be dependent on the ratio of the two DIBs, while 5850 Å feature seems to be well-correlated with 5797 Å DIB.

In 2000, Walker, Bohlender and Krełowski published an article about a possible isotopic structure of 5797 Å and 6614 Å bands. They were observing 6 stars with a very high-resolution ($R = 60\,000 - 120\,000$) spectrograph and the detailed structures of the two DIBs were revealed. The features were simulated by bands composed of several lines which corresponded to possible isotopic shifts of large carbon molecules – the isotopic model which they used was developed by Webster (1996). The results show that the match was good for 5 of the 6 observed stars and the team pointed out that carriers of these bands are supposed to be highly symmetrical and possibly spherical.

The two bands, 5780 Å and 5797 Å, were also observed by Weselak et al. (2008). This team measured equivalent widths of the two DIBs and column densities of CH and CN molecules. Results showed that correlation of DIBs with the CH molecule is better than with the CN molecule. This leads to the suggestion that carriers of these bands might be hydrocarbons.

1.1.2 6196 Å and 6614 Å – The Well-Correlated DIBs

The 6196 **Å** and 6614 **Å** bands have the closest relation among all of the DIBs. McCall et al. (2010) found a correlation coefficient of 0.986 which suggests a common carrier, in which case the difference between calculated and a perfect correlation should be due to the errors of methods used (e.g. uncertainty of continuum placement) or due to the presence of other lines (blending). On the other hand, if these two DIBs do not share the same carrier, the correlation coefficient at least tells us that the two carriers have to be very similar. Throughout the whole published data set, the ratio of the equivalent widths seems to be $W6614/W6196 \sim 4$.

The profile of 6614 Å band was discussed by Marshall, Krełowski and Sarre (2015). They observed spectra of two stars with resolution power $R \sim 115\,000$. They proposed

that the profile of the band could be explained by vibrational (or electronic) bands of a molecule similar to the polycyclic aromatic hydrocarbons (or PAHs). The observed difference in the shape of the band between the two lines of sight was interpreted as a difference between the order of internal excitation. The research team also looked back at work done by Oka et al. (2013) where the observation of an extended red tail of the band is mentioned. Oka explained this phenomenon to be due to polar molecules with highly populated rotational levels maintained by near infrared source. Marshall, Krełowski and Sarre explained the presence of the red tail as the possible result of the vibrational hot bands.

Galazutdinov et al. (2002) studied the 6196 Å band profile in different lines of sight. The profile of the band was narrow in some lines of sight while in other, it was broad and contained additional features. This could be, for example, due to the presence of the ^{13}C carbon isotope. Another explanation was based on the studies of Kazmierczak et al. (2009) who proposed a relation between the strength of 6196 Å DIB and excitation temperature of C_2. They argue that the carrier of this band could be a centrosymmetric molecule with its spectral bands broader at higher rotational temperatures – this would rule out polar molecules as possible carriers due to the efficient cooling by rotational emission of such molecules.

1.1.3 4430 Å DIB and 2175 Å Absorption Bump

The absorption band at 4430 Å is an interesting feature. It is one of the broadest DIBs observed and is arguably the most researched one of them. For example, Ehrenfreund et al. (1992) searched for 4430 Å DIB in the spectra of two polycyclic aromatic hydrocarbons – coronene and ovalene. However, investigation of the spectra of these molecules showed bands which are not close to any of DIBs.

A possibility of a common carrier of 4430 Å and 7565 Å DIBs was studied by Léger et al. (1995). This team was responsible for one of the first possible laboratory identifications of DIBs. They used UV radiation on the 1-methyl-pyrene molecule which showed absorption features near the mentioned DIBs. Unfortunately, the experiment was made with the molecule in a neon matrix for which the matrix shifts could not be measured, but were estimated instead. Results of this experiment also predict a perfect correlation between intensities of the two DIBs in different lines of sight, however, this has not been observed, yet.

Mostly during the 1970s, it was commonly believed that 4430 Å band arises from mantles of small interstellar dust grains. Nandy and Thompson (1975) observed spectra of over 60 stars and found that 4430 Å DIB is well correlated with an absorption feature present near 2200 Å. This phenomenon was also investigated by Witt et al. (1983) by looking at the correlation of the 2175 Å extinction bump and $A(4430)/E(B-V)$ ratio. In this case, correlation coefficients were found to be low (< 0.6) with quite high uncertainties. Later it was suggested by Krełowski et al. (1987) that while the 4430 Å feature arises from the mantle of dust grains, the 2175 Å feature should be the result of the existence of dust grain cores.

Isobe et al. (1986) presented observations of 800 O- and B-type stars. They were able to use 482 spectra of these stars to find strengths of the 4430 Å feature. Results confirmed

what was suggested in the late 1970s – the strength of this band in not perfectly correlated with the extinction at any given line of sight and therefore it does not depend solely on the abundance of dust grains.

1.2 Properties of DIBs

There are several common properties of all DIBs which have been briefly summarized by Snow & Destree (2011).

- Diffuse interstellar bands are generally very narrow and weak features. Most of them have full width at half maximum of their intensity well below 10 Å. The only well-researched exception is the DIB at 4430 Å which can be ~ 20 Å broad. All of the DIBs have peak intensity of absorption $< 30\%$ of the continuum intensity.
- The appearance of different sets of DIBs seems to be connected to different densities of interstellar clouds found between us and the observed stars.
- There is a good correlation between the strengths of diffuse interstellar bands and colour excess $E(B-V)$ which is used to measure the extinction.
- Carriers of the DIBs seem to be part of the diffuse medium (neutral hydrogen, ionized hydrogen or hot coronal gas) rather than part of the molecular clouds.
- They usually have asymmetric profiles, with the exception of some of the broad DIBs.
- In the case of some diffuse interstellar bands, very-high-resolution spectroscopy revealed detailed structure of their profiles. This is usually associated with rovibrational bands.
- DIBs do not show any sign of polarization. This tells us that the carriers are most likely not connected to interstellar dust, since dust grains are thought to be aligned under the influence of interstellar magnetic fields and in such conditions, the polarization of light would occur.
- DIBs found in the UV region of the spectrum are by far weaker than the 4430 Å DIB.

It is important to point out that although the DIBs are usually absorption features, they were also possibly observed as emission features towards, at least, one object, the Red Rectangle Nebula (Sarre et al. 1995). It is also worth mentioning that the correlation between the strength of DIBs and $E(B-V)$ is often statistically not significant – coefficients tend to be below 0.7 and errors might not even be mentioned. The information we get from these correlations is that there is a relation between DIBs absorption and the colour excess in a given region but there is a systematic spread in the colour excess. An example of this can be seen in Figure 1.2.

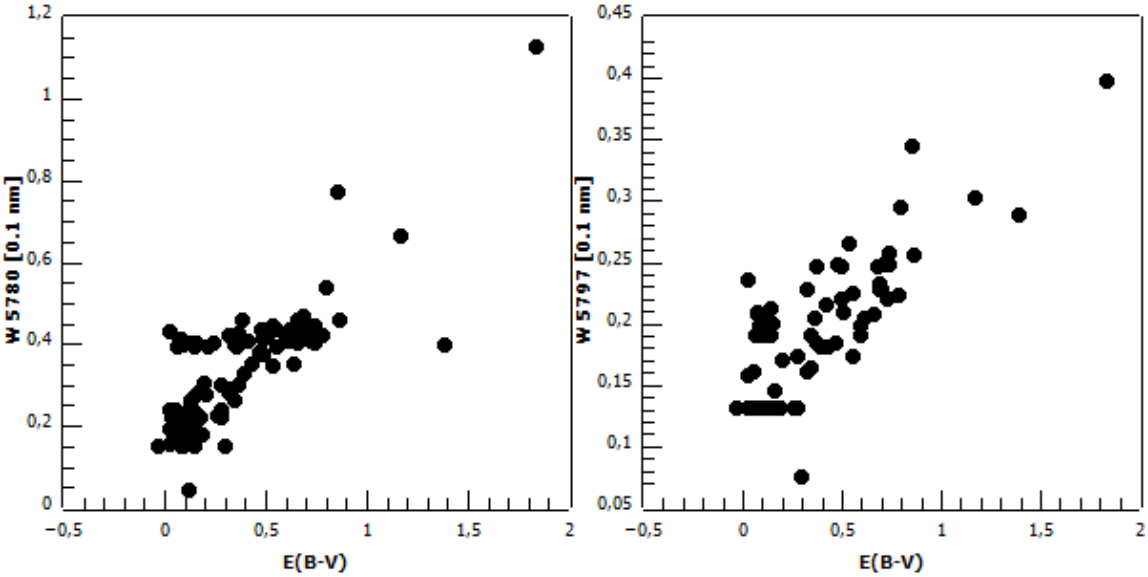

Figure 1.2: Correlations between equivalent widths of DIBs and the colour excess $E(B-V)$, data from Snow et al. (1977).

1.3 Carriers of DIBs

What is the carrier of the DIBs? This question remains unanswered since the day the DIBs were discovered but some recent experiments suggest that we may be on a good track. There are some facts we know about the carrier:

- Carrier of DIBs is not an atom nor a simple molecule such as H_2 or OH.
- The hypothesis of multiple carriers seems to be more likely than just one common carrier.
- The molecule which is responsible for DIBs should contain C-C and C-H bonds.
- Carrier of DIBs is most likely a polycyclic aromatic hydrocarbon (PAH) or a large carbon structure (e.g. a fullerene).

Wdowiak (1980) gives one of the first published laboratory experiments with the aim to investigate a possible carrier of the DIBs. He was using a mixture of methane in argon matrix which he excited using plasma discharge in a discharge tube. He was able to produce features at wavelengths close to some of the strong DIBs but unfortunately, the results were inconclusive.

Over the course of the last 30 years, a large number of molecular species was investigated in laboratory experiments with similar methods as Wdowiak used. The possibility of relatively simple ions of carbonic chains C_2, C_3 and C_7 being carriers was already dismissed but more research is required. Basic organic compounds which are confirmed to be present in the interstellar medium were also examined – methane, molecules from the methyl group, cyclopropenylidene and others. Even experiments with PAHs did not bring positive results so far (for example Ehrenfreund et al. 1992). Recently, however, a laboratory assignment of two DIBs was made to a large molecule ion C_{60}^+ (Campbell et al. 2015).

1.3.1 Polycyclic Aromatic Hydrocarbons

Polycyclic aromatic hydrocarbons form a group of large organic compounds, resistant to UV dissociation, with at least two fused aromatic rings. Their presence in the interstellar medium can be confirmed by their spectral signatures between 3 and 12 microns. They were and still are studied intensively and some works provide a general description of their importance in the interstellar medium. Information gathered here was mostly taken from the article by Verstraete (2011).

PAHs are believed to be an important heating component of the interstellar medium. Since their presence is marked by a UV radiation field, PAHs may lose electrons via photoelectric effect. They also show strong absorption features at 700 Å and 2000 Å – they could be the source of the 2175 Å extinction.

These molecules are good candidates for explaining the formation of interstellar molecular hydrogen gas. The precise mechanism of H_2 formation is not very well known but it is supposed to happen on the surface of dust grains. Moreover, PAHs are expected to represent a large fraction of the surface of dust grains. One can, therefore, conclude that H_2 formation is most likely related to the presence of PAHs – this relation was, to some degree, confirmed by observations.

Containing electrons which are easily polarized, PAHs may serve for capturing electrons from the medium. As an important part of the dust grains, they are believed to be quite abundant in the dense gas and can be present also in regions shielded from external UV radiation. Within these regions, negative PAH-ions can be very abundant. Outside of these regions, less abundant PAH-ions can be negatively or positively charged which may lead to the clustering of PAHs.

Salama et al. (2011) made a comparison of spectra of ten PAHs with observed spectra of reddened stars. None of the PAHs could be assigned to DIBs, but a comparison of the band profiles of both species led to the discovery of certain similarities. This, however, requires a careful approach – there is a large difference between interstellar and laboratory conditions.

1.3.2 Fullerenes

The existence of fullerenes was experimentally confirmed in 1985 by a group of scientists. Harry Kroto, Richard Smalley, and Robert Curl irradiated graphite disk by laser ($\lambda = 532$ nm) in short 5 ns pulses. A presence of helium gas above the vaporization zone was required for the process of formation of clustering of vaporized species and it carried these clusters along to the mass spectrometer. The team determined that the detected molecule of sixty carbon atoms (among other carbon molecules) formed a truncated icosahedron – this shape very well resembles the shape of a football (soccer ball).

Kroto and other scientists further studied fullerenes. They all found that these molecules are very stable. Kroto (1987) presented empirical rules which related the stability of fullerenes to the presence of pentagonal rings, based on the prediction that fullerenes have closed cage structure. These rules predicted that the most stable fullerenes should be C_{24}, C_{28}, C_{32}, C_{36}, C_{50}, C_{60} and C_{70} – this was readily compared with observation and confirmed.

Wave-particle duality of light is a well-known phenomenon. It was proposed by de Broglie that massive particles, like electrons, should also possess both particle and wave properties. This was experimentally tested and confirmed. An interesting experiment was done by Arndt et al. (1999) who observed de Broglie wave interference of C_{60} molecules. C_{60} is one the largest particles known to display both particle and wave-like behaviour.

Fullerenes show great promises in medical applications (Bakry et al. 2007). The utilization in medicine is based on the cage structure and stability of these molecules. For example, there are attempts to use C_{60} fullerene for agent transportation in the human body.

The presence of fullerenes in the interstellar medium was proposed as soon as they were discovered. The reason is the existence of unexplained DIBs that require the carrier to be abundantly present in the interstellar medium. Such a carrier has to be very resistant, mostly to photodissociation. Some fullerenes have this property and their spectra were studied in laboratories. When compared with spectra of observed stars, bands of fullerenes coincided with several structures in the spectrum. Mostly known are their vibrational spectra in IR between 5 and 20 μm. Iglesias-Groth (2004) studied the possibility of fullerenes being responsible for UV extinction bump. She found that several large fullerenes (C_{1500}, C_{2160}, C_{2940} and C_{3840}) could reproduce the UV bump, however, formation and existence of such large molecules in the interstellar medium was not explained. Estimation of the amount of carbon in fullerenes leads to the prediction that they carry about $1/5$ of the total number of carbon atoms in the diffuse interstellar medium.

The carrier of two DIBs in the $9000 - 10\,000$ Å region was predicted already in the late 90s to be the C_{60} molecule – its spectral features in the near-infrared part of the spectrum coincided with observed DIBs. Results of the further experiments will be discussed in Chapter 4.

Chapter 2

Molecular Spectroscopy

Interstellar medium contains a large number of different molecules. Although not as abundant as atoms, their presence is very important for the chemical evolution of the medium. Furthermore, observing spectral lines of molecules brings us more information about the characteristics of the studied regions of space. At first, only simple molecules, such as CH, CN, CO and other were confirmed to be part of the interstellar medium. However, as the quality of spectra has been increasing, we were able to find more complex spectral features. This lead to the discovery of larger interstellar organic and inorganic species. Being largest known particles of the interstellar gas, PAHs and fullerenes are the best example of such molecules.

States of molecules (and atoms) can be described by wavefunctions and corresponding energy levels. A transition between two energy levels means that the system must have emitted or absorbed light of frequency ν given by the well-known relation

$$E = h\nu. \tag{2.1}$$

Such process makes spectral lines appear in spectra of observed objects. Because of the unique nature of their energy levels, the presence of molecules in the studied medium can be determined by investigating the wavelengths of their characteristic spectral lines.

It is not practical trying to find precise mathematical expressions for states of molecules, especially for larger ones. Therefore, simplifications are required when solving such problems. A common way of dealing with this is to use the Born-Oppenheimer approximation which utilizes the fact that the atomic nuclei are much heavier than electrons. This gives us the possibility to treat nuclear and electronic states separately. We will focus mainly on the states of nuclei but electronic transitions will be briefly described as well.

In molecular spectroscopy, one usually deals with spectral features in radio, infrared or microwave regions of the electromagnetic spectrum. Individual atoms which form a molecule are not stationary – they oscillate, while, as a whole, the molecule rotates. These two types of motion are used to find states and energy levels of molecules. Mathematical models that are commonly used to describe vibrational and rotational states are based on the harmonic oscillator and on the rotation of a rigid body.

2.1 Electronic Spectra

The motion of electrons in a molecule is the most complicated part one has to deal with in molecular spectroscopy. The transition between two states corresponds to the excitation or deexcitation of an electron. As excited electron moves to higher energy levels, the bond with the nuclei gets weaker which results in the change of the curve of the potential energy function of the molecule. The energy difference between the minima of the two potentials is then the electronic energy and is typically denoted T_e. There is no particular mathematical model that describes electronic states of molecules. Instead, their spectra are experimentally observed and listed in tables.

2.2 Vibrational Transitions

Each molecule has a certain number of vibrational modes. They are unique for each molecule and can be used to calculate the energy of their vibrational states. Generally, a molecule consisting of N atoms has a total number of $3N-6$ vibrational degrees of freedom but symmetries will result into a lower number of observed modes. For example, the complex structure of fullerene C_{60} has 174 degrees of freedom while only 46 vibrational frequencies were observed in a laboratorial environment. The simplest description of an oscillating molecule is a diatomic molecule that has only one mode. Although very simple, calculations that will be mentioned in this section can be extended to even more complex molecules, if we take into account their symmetries.

A harmonic oscillator is the most elementary model of vibration of diatomic molecules which has a quadratic form. However, this works only as a first approximation. A quartic potential (a simplified case of the Morse potential) can be used to describe the atomic motion more precisely. Finally, when working with large molecules, even a more complicated potential must be used. Later in this work, we will be interested only in oscillating carbon atoms. Experimentally, it was shown that Brenner and Tersoff potentials are the best choices for describing such systems.

2.2.1 Harmonic Oscillator

In quantum mechanics, the Hamiltonian of the one-dimensional linear harmonic oscillator is

$$\hat{H} = \frac{\hat{p}^2}{2m} + \frac{1}{2}m\omega^2\hat{x}^2\,, \tag{2.2}$$

where m is the mass of the particle, ω is the angular frequency of the oscillator, and position $\hat{x}$ and momentum $\hat{p}$ operators are

$$\hat{x} = x\,, \tag{2.3}$$

$$\hat{p} = -i\hbar\frac{\partial}{\partial x}\,. \tag{2.4}$$

We want to find energy the eigenvalues of such system. Solving the time-independent Schrödinger equation is a possible way of dealing with this problem. However, it can be much more simple (and elegant) to define the dimensionless ladder operators

$$\hat{a} = \sqrt{\frac{m\omega}{2\hbar}}\hat{x} + i\sqrt{\frac{1}{2m\hbar\omega}}\hat{p}, \tag{2.5}$$

$$\hat{a}^\dagger = \sqrt{\frac{m\omega}{2\hbar}}\hat{x} - i\sqrt{\frac{1}{2m\hbar\omega}}\hat{p}, \tag{2.6}$$

which are also sometimes called annihilation and creation operator, respectively. By rewriting position and momentum in terms of ladder operators, we will find the Hamiltonian in the form

$$\hat{H} = \hbar\omega\frac{1}{2}\left(\hat{a}\hat{a}^\dagger + \hat{a}^\dagger\hat{a}\right). \tag{2.7}$$

Operators $\hat{a}$ and $\hat{a}^\dagger$ are not Hermitian but it can be shown that they are Hermitian adjoint

$$[\hat{a}, \hat{a}^\dagger] = \hat{1}. \tag{2.8}$$

Furthermore, we can notice that

$$[\hat{a}^\dagger\hat{a}, \hat{a}] = -\hat{a}, \tag{2.9}$$

$$[\hat{a}^\dagger\hat{a}, \hat{a}^\dagger] = \hat{a}^\dagger, \tag{2.10}$$

$$[\hat{a}^\dagger\hat{a}, \hat{H}] = \hat{0}, \tag{2.11}$$

meaning that $\hat{a}^\dagger\hat{a}$ and $\hat{H}$ commute and have a set of joint eigenstates which we will denote $|n\rangle$. We will let $\hat{a}^\dagger\hat{a}$ and $\hat{H}$ operate on these states and find energy eigenvalues

$$\hat{a}^\dagger\hat{a}\,|n\rangle = n\,|n\rangle\,, \tag{2.12}$$

$$\hat{H}\,|n\rangle = E_n\,|n\rangle = \hbar\omega\left(n + \frac{1}{2}\right)|n\rangle\,, \tag{2.13}$$

$$E_n = \hbar\omega\left(n + \frac{1}{2}\right), \tag{2.14}$$

where $n \geq 0$. The corresponding eigenfunctions $\psi_n(x)$ corresponding to the given eigenstate $|n\rangle$ can be calculated

$$\psi_n(x) = \frac{1}{\sqrt{\sqrt{\pi}2^n n!\, x_0}}\, e^{\frac{-x^2}{2x_0^2}}\, H_n\left(\frac{x}{x_0}\right), \tag{2.15}$$

where H_n are the Hermitian polynomials

$$H_n(y) = (-1)^n\, e^{y^2}\, \frac{\mathrm{d}^n}{\mathrm{d}y^n}\left(e^{-y^2}\right). \tag{2.16}$$

Although relatively simple, solutions of this problem are very important in molecular spectroscopy. The relation for energy eigenvalues of a one-dimensional harmonic oscillator can also be derived for a three-dimensional case. Furthermore, we would arrive at similar results if we were dealing with a system consisting of more particles, but this work does not cover the second quantization which is usually used when considering such problems.

Let us take a closer look at the discrete set of energies of an oscillator. It is obvious that the lowest state the molecule can occupy has a non-zero energy. Due to the nature of electric dipole moment in the harmonic oscillator approximation, the only transitions allowed are $\Delta n = \pm 1$ which means that energies are equally spaced. However, it is important to note that this model of molecular vibration has several flaws. First of all, by plotting potential energy of a harmonic oscillator against internuclear distances, the potential of such system is found to be described by a parabola. It is known that this is a good fit to a real potential only in the case that the molecule is in the lowest vibrational states. Moreover, harmonic oscillator gives for $n \to \infty$ energies $E_n \to \infty$ but in reality, if enough energy is given to a diatomic molecule, the bond between atoms is broken and the molecule dissociates.

Evidently, more complicated models are required to properly depict the motion of vibrating molecules, but it is clear that the quadratic potential of a harmonic oscillator is good enough as a first approximation. A general polynomial can be used to get better results, with the quadratic term being of the highest order.

2.2.2 Anharmonic Oscillators

The most simple example of anharmonic motion of two bound atoms is characterized by the Morse potential

$$V(x) = D_\mathrm{e}\left(1 - e^{-\alpha x}\right)^2 , \tag{2.17}$$

$$x = \frac{r - r_0}{r_0} , \tag{2.18}$$

where r is the internuclear distance, r_0 is the equilibrium distance, α is a constant (but varies for each molecule), and D_e is the dissociation energy. It is worth noting that D_e is different from the energy required for dissociation D_n – even in the lowest state, energy of the system is non-zero and the relation between the two energies is

$$D_n = D_\mathrm{e} - E_n . \tag{2.19}$$

The whole potential can be well approximated by a fourth-degree polynomial. We can find it by expanding the exponential into Taylor series around the minimum, so that we get

$$V(x) \approx D_\mathrm{e}\left(\alpha^2 x^2 - \alpha^3 x^3 + \frac{7}{12}\alpha^4 x^4\right) . \tag{2.20}$$

Since the first term resembles a harmonic oscillator and the other terms are of lower order, the first order perturbation theory can be used to calculate corrections to energies found in the harmonic case. Energy eigenvalues for the Morse potential are found to be

$$E_n \approx \hbar\omega\left(n+\frac{1}{2}\right) - \frac{\hbar^2\omega^2}{4D_\mathrm{e}}\left(n+\frac{1}{2}\right)^2. \tag{2.21}$$

If we had taken a higher degree polynomial, we would have found that even more precise solutions exist,

$$E_n = \hbar\omega\left(n+\frac{1}{2}\right) - \hbar\omega\varepsilon_1\left(n+\frac{1}{2}\right)^2 + \hbar\omega\varepsilon_2\left(n+\frac{1}{2}\right)^3 - \ldots, \tag{2.22}$$

but the approximate values from equation 2.21 are typically sufficient for spectroscopical purposes. If not, a more fitting potential must be chosen.

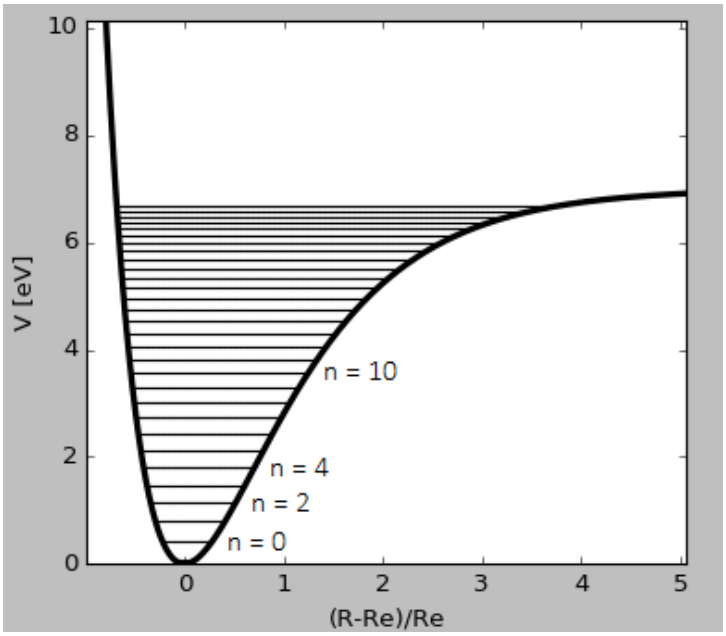

Figure 2.1: The Morse potential. Thin horizontal lines represent the individual energy eigenvalues.

Several important comparisons can be made between the quadratic and Morse potential. Firstly, it can be instantly seen in Figure 2.1 that energy levels in the case of the Morse potential are not evenly spaced but their density rises as n gets larger. Another difference is between the selection rules – there are generally none but, in practice, the situation depends on the conditions in the interstellar medium. Finally, despite all advantages of the Morse oscillator, both potentials are inadequate if the vibrational quantum number n is large.

Brenner and Tersoff potentials are the best options when studying molecules which contain only carbon and hydrogen atoms. Because of their complex, but very similar form, we will only have a brief look at one of them.

In 1990, Brenner published an article in which he described an empirical many-body potential based on the Tersoff's work done two years prior to this. It was proposed that it can be used for molecular-dynamics simulations and was since then adapted by several software programmes. Being expressed by 10 independent parameters (two sets were taken from Kaur et al., 2007, and listed in Table 2.1), the potential consists of the sum of a repulsive

Table 2.1: Two examples of parameters used in the Brenner potential.

Parameter	Set 1	Set 2
D_e [eV]	6.325	6.0
S	1.29	1.22
β [Å^{-1}]	1.5	2.1
R_e [Å]	1.315	1.39
R_1 [Å]	1.7	1.7
R_2 [Å]	2.0	2.0
δ	0.80469	0.5
a_0	0.011304	0.00020813
c_0	19	330
d_0	2.5	3.5

(V_R) and an attractive term (V_A). In order to limit its range only to the closest atoms, these terms are further multiplied by a cut-off function f_{ij}. The total potential energy of N nuclei is then the sum over all contributions and depends on the equilibrium internuclear distance r_{ij} between any two atoms

$$V = \sum_{i=1}^{N} \sum_{j>i}^{N} f_{ij}(r_{ij}) \left(V_R(r_{ij}) - \bar{B}_{ij} V_A(r_{ij}) \right) , \tag{2.23}$$

where $\bar{B}_{ij}$ is an empirical bond-order function and all the individual functions are calculate as follows:

$$f_{ij}(r_{ij}) = \begin{cases} 1 & \text{if } r_{ij} < R_1 \\ 1 + \cos \frac{\pi(r_{ij}+R_1)}{R_2-R_1} & \text{if } R_1 < r_{ij} < R_2 \\ 0 & \text{if } r_{ij} > R_2 \end{cases} , \tag{2.24}$$

$$V_R(r_{ij}) = \frac{D_e}{S-1} e^{-\sqrt{2S}\beta (r_{ij}-R_e)} , \tag{2.25}$$

$$V_A(r_{ij}) = \frac{D_e S}{S-1} e^{-\sqrt{\frac{2}{S}}\beta (r_{ij}-R_e)} , \tag{2.26}$$

$$\bar{B}_{ij} = \frac{B_{ij} + B_{ji}}{2} , \tag{2.27}$$

$$B_{ij} = \left(1 + \sum_{k}^{N} G(\theta_{ijk}) f_{ik}(r_{ik}) \right)^{-\delta} , \tag{2.28}$$

$$G(\theta_{ijk}) = a_0 \left(1 + \frac{c_0^2}{d_0^2} - \frac{c_0^2}{d_0^2 + \left(1 + \cos\theta_{ijk}\right)^2} \right) . \tag{2.29}$$

Although this model seems to work very well and is useful for many simulations, calculating energy states from so complicated Hamiltonian is extremely difficult. Let us

take an example – the C_{60} molecule. Even though the potential can be expanded into a (very high degree) polynomial, the summation over all particles may present a problem when attempting to work with the perturbation theory. A direct solution of the Schrödinger equation is impossible as there appears to be no software capable of calculating energy eigenvalues of quantum systems so large. It may be possible to use trial-and-error method in order to find a solution to the Schrödinger equation, but no numerical method is fast enough to do so without using supercomputers.

To sum up, Morse potential is most likely the best approximation that can be readily used for the description of vibrational states of molecules, despite the fact that better models are available. It is possible that the second quantization may present a good way of getting to the solution but such attempt is beyond the scope of this work.

2.3 Molecular Rotation

Computations of the rotational energy levels of diatomic molecules yield good results when working with the model of a rigid rotor. Nuclei of molecules are regarded as point masses connected by a rigid bond and rotate around an axis through the centre of the mass of the system. If we use spherical coordinates and assume that the wave function can be split into a radial and an angular part, we are able to find rotational energies with the use of spherical harmonic functions

$$E_J = \frac{\hbar^2}{2\mu R^2} J(J+1)\,, \tag{2.30}$$

where μ is the reduced mass of the molecule, R is the internuclear separation (or bond length) and J is the rotational angular momentum quantum number with values $J \geq 0$. In spectroscopy, a more compact form of this equation is typically used

$$E_J = BJ(J+1)\,, \tag{2.31}$$

$$B = \frac{\hbar^2}{2\mu R^2}\,, \tag{2.32}$$

with B being the so-called rotational constant. However, the real molecule oscillates and that results into B not being actually constant since it depends on R which changes. In order to calculate B, equilibrium internuclear distance R_e is used instead of R. Furthermore, the centrifugal force, which appears in such rotating system, can stretch the bond between nuclei – rotational constant is then smaller and correction terms are needed to account for the change in energies

$$E_J = BJ(J+1) - DJ^2(J+1)^2 + \dots\,, \tag{2.33}$$

$$D = \frac{\hbar^4}{2\mu^2 k R_\mathrm{e}^6}\,, \tag{2.34}$$

where k depends on the oscillation and is called the force constant.

Besides the rigid rotor which has two non-zero principal moments of inertia ($I_A = 0$, $I_B = I_C$), three other models are used to describe the rotation of larger molecules. In the case of all principal moments of inertia being the same, energy levels are calculated precisely as previously and such molecules are designated as spherical top. If $I_A < I_B < I_C$ and all values are different from zero, we are dealing with asymmetric top molecules and calculations are non-trivial since neither one, nor two rotational quantum numbers are sufficient. The only exception is the situation when $I_A < I_B = I_C$ with $E(J,K)$ that corresponds to symmetric top molecules.

As it was mentioned before, rotational motion depends on the vibrational motion. This fact means that the separation which we have done is not feasible. However, we can use these results to create a unified rovibrational model. In the case of a Morse potential and a rigid rotator, the energy levels can be calculated as follows

$$E(n,J) = \hbar\omega\left(n+\frac{1}{2}\right) - \frac{\hbar^2\omega^2}{4D_\mathrm{e}}\left(n+\frac{1}{2}\right)^2 + BJ(J+1) - \frac{\hbar\,\omega B}{2D_\mathrm{e}}\left(n+\frac{1}{2}\right)J(J+1)\,, \tag{2.35}$$

where the last term accounts for the connection between the two motions. Such energy states give rise to the rovibrational spectrum of a molecule and its existence is observationally confirmed. These spectral lines form into bands which can be resolved in the case of small molecules. On the other hand, if a molecule is large enough, rotational lines of such species tend to be grouped closely together and it may not be possible to resolve them individually. However, their existence can still be confirmed thanks to the specific structure of rovibrational bands.

The structure of the band consists of three parts. The first one is labelled as a Q-branch which corresponds to the transition $\Delta J = 0$ and is located at the band origin. This branch has a very high but thin peak since all such transitions lie at the band origin. P- and R-branches are the result of transitions $\Delta J \neq 0$ and are located at lower and higher frequencies, respectively. They tend to have lower maximum intensities than the Q-branch, but this is compensated by the number of possible transitions to lower/higher states – this makes them appear wider in the spectrum. Furthermore, the internuclear equilibrium distance used for the calculation of rotational energies is increased at higher vibrational frequencies (in the case of an anharmonic oscillator). This results in the broadening of the P-branch while the R-branch gets narrowed. Overall, the appearance of such structures may differ and they usually do not quite resemble what is shown in the spectrum in Figure 2.2.

2.4 Population of Energy Levels

The Boltzmann distribution can only rarely be used in astrophysics when studying a medium. The reason for this is that it requires the medium to be in the thermodynamic equilibrium – such condition is usually not satisfied in stellar atmospheres, for example. However, if we consider the condition of local thermodynamic equilibrium (LTE) in an interstellar environment, we should be able to use (limitedly) the Boltzmann distribution. Let us say that N is the number of possible states a molecule can occupy, T is the temperature of the system of molecules and E_i is the energy level of the given state. The probability that

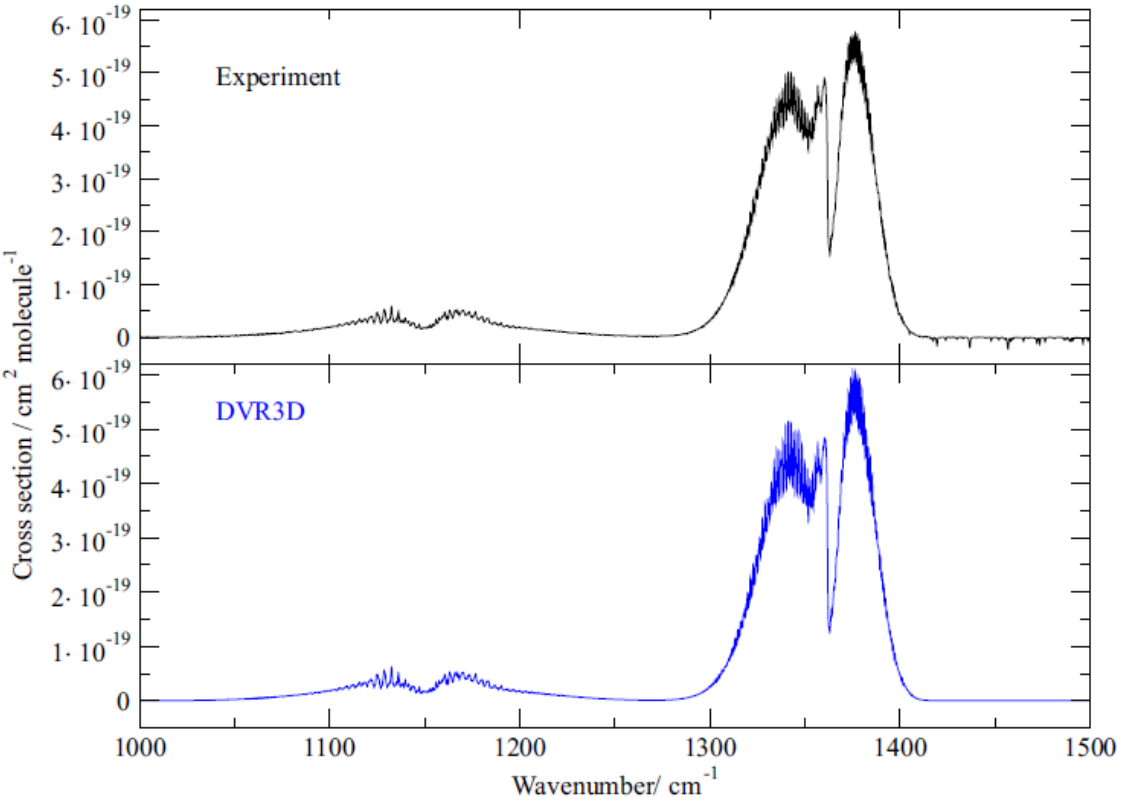

Figure 2.2: Experimentally obtained rovibrational spectrum of the molecule SO_2 by Underwood et al. (2016).

a molecule occupies the state i (with a degree of degeneracy g_i) is

$$P_i = P_0 \frac{g_i}{g_0} e^{-\frac{E_i - E_0}{k_B T}} . \tag{2.36}$$

We have taken the ratio of the studied state and the ground state in order to avoid the calculation of the partition function. The degrees of degeneracy of vibration and rotation differ. If we have a look at pure harmonic oscillations, we are working with the degeneracy factor $g_i/g_0 = 1$, so we get

$$\frac{P(n)}{P_{0,n}} = e^{-\frac{\hbar\omega n}{k_B T}} . \tag{2.37}$$

On the other hand, a heteronuclear rigid rotator has $g(J) = 2J+1$. This time, the probability is not an exponential function of the quantum number but instead, we have a Gaussian function

$$\frac{P(J)}{P_{0,J}} = (2J+1)\, e^{-\frac{BJ(J+1)}{k_B T}} . \tag{2.38}$$

It is immediately obvious that the probability of finding a harmonic oscillator in the state i is highest at $n = 0$. In the case of a rigid rotator, the maximum of the distribution is located at

$$J_{\max} = \sqrt{\frac{k_B T}{2B}} - \frac{1}{2}, \tag{2.39}$$

which can be as high as $J = 500$. The main difference between these two distributions is that even at very low temperatures ($T < 50$ K), more than one rotational level is occupied by a significant number of molecules of given species. On the contrary, only the ground (and possibly the first excited) vibrational state would be populated at such temperatures. A different result can be obtained by choosing the Morse oscillator, for which the distribution $P(n,J)$ once again resembles the Gaussian function.

2.5 Isotope Effect

The presence of various isotopes is extremely important in spectroscopy. Their presence greatly changes the spectrum of a molecule by shifting the bands. This effect is very apparent in the case of diatomic molecules but can also be observed for polyatomic molecules. As we have seen in the equation 2.32, the rotational constant depends on the reduced molecular mass. If a heavier isotope of an atom is present (for example, HD instead of H_2), the energy states of such system will slightly shift towards lower values. These shifts are much larger in the case of vibrations. A particle with higher mass will cause a change in the vibrational modes. As a result, the frequencies corresponding to rovibrational transitions are lowered. The ratio of intensities of the original and shifted bands depends on the relative abundance of the given isotopes.

Isotope effect may serve us as a spectroscopical tool for finding the ratio of isotopes. However, its existence can also be used for the purposes of this work. Let us presume that we have found a certain amount of molecular bands which have an unknown carrier. If we suspect a certain molecule is responsible, we can create a model that can be used to calculate its spectra. In the case that some of the bands match observed spectrum, an isotopic shift can be calculated and searched for. Supposing that the model is accurate enough, this could provide the desired proof of the existence of such molecular species in the ISM. Moreover, the value of the ratio of isotopes $^{13}C/^{12}C$ depends on the location in the ISM where the molecules are located. This can be used to test which phase of the medium the bands originate from.

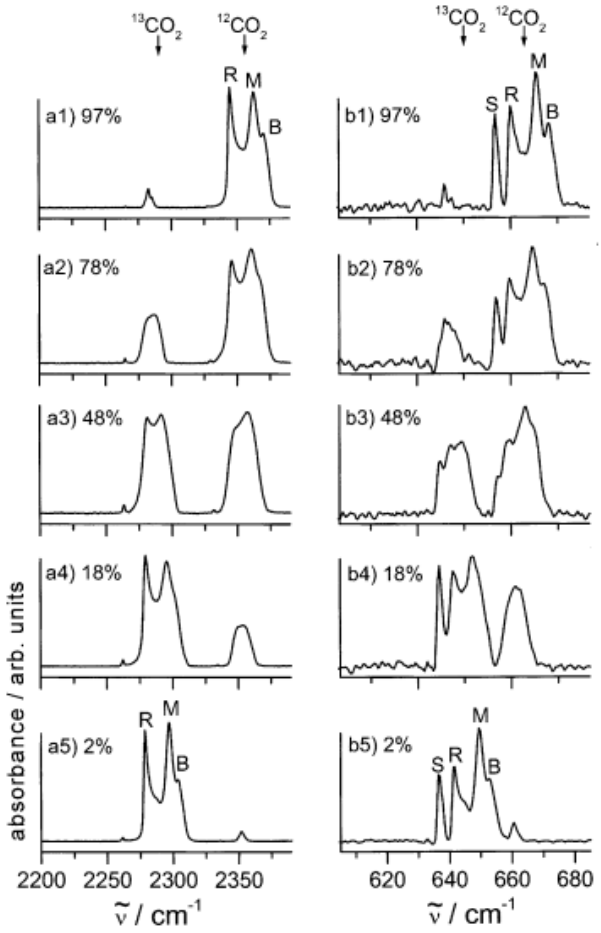

Figure 2.3: Isotope effect seen in the infrared spectra of CO_2 with the ratio $^{12}CO_2/^{13}CO_2$ shown in each panel. Taken from Signorell & Kunzmann (2003).

Chapter 3

Diffuse Interstellar Medium

The interstellar medium (ISM) is everything we can find in the space between stars – electromagnetic radiation, gravitational fields, baryonic matter, dark matter, etc. In this work, we will be dealing only with the baryonic matter which is almost entirely composed of hydrogen and helium. Despite this fact, it is very important to know abundances of other atoms and molecules as they strongly influence our models of stellar and even Galactic evolution.

When talking about the ISM, most people will imagine giant molecular clouds within which stars are born. Although these large self-gravitating objects contain most of the mass of interstellar baryonic matter, they only occupy a very small fraction of the whole volume of our Galaxy. The rest of the baryonic matter is contained within the interstellar dust and diffuse interstellar gas (densities at or below 10^2 particles per cubic centimetre) – these fill most of the volume of the interstellar and intergalactic medium.

Studies of the ISM indicate that it is important to know physical conditions within studied regions. It was shown that the baryonic matter of the ISM can be divided into several phases based on the particle density n_{H} and temperature T of the gas. We will use the interpretation of phases of the ISM described by Bruce T. Draine:

- Dense molecular gas – $n_{\mathrm{H}} \sim 10^3 - 10^6$ cm^{-3} , $T \sim 10 - 50$ K
- H II regions – $n_{\mathrm{H}} \sim 10^4$ cm^{-3} , $T \sim 10^4$ K
- Stellar outflows – $n_{\mathrm{H}} \sim 1 - 10^6$ cm^{-3} , $T \sim 50 - 1000$ K
- Diffuse molecular gas – $n_{\mathrm{H}} \sim 100$ cm^{-3} , $T \sim 50$ K
- Cold neutral medium (CNM) – $n_{\mathrm{H}} \sim 30$ cm^{-3} , $T \sim 100$ K
- Warm neutral medium (WNM) – $n_{\mathrm{H}} \sim 10^{-1}$ cm^{-3} , $T \sim 5000$ K
- Diffuse H II gas (warm ionized medium) – $n_{\mathrm{H}} \sim 0.1 - 1$ cm^{-3} , $T \sim 10^4$ K
- Hot ionized medium (HIM, or coronal gas) – $n_{\mathrm{H}} \sim 0.004$ cm^{-3} , $T > 300\,000$ K

The DIBs are usually observed in the lines of sight which are not obstructed by dark clouds. This means, that most of the time we are dealing with the diffuse parts of the ISM.

For the purpose of this work, we will not deal with the dense molecular gas and H II star forming regions where densities are relatively high. Instead, we will discuss the properties of the remaining low-density phases.

3.1 Neutral Medium

Filled mostly with neutral atomic gas, the neutral medium is mostly observed at longer wavelengths, where the H I 21 cm hyperfine structure line is present – this is also the cooling source of the medium. Depending on the temperature and density of the gas, we can talk about warm (WNM) and cold (CNM) neutral medium.

Cold neutral medium is mostly concentrated in clouds with densities ~ 10 cm^{-3} and temperatures ~ 100 K. These clouds are relatively easily observed at 21 cm absorption line (high optical depth) in the lines of sight towards extragalactic radio sources. Temperatures of the cold gas clouds are well determined and checked by observation of other parts of the spectrum, see for example Roy et. al (2006).

Warm H I gas has densities $\sim 0.01 - 1$ particles per cubic centimetre and temperatures of $1000 - 8000$ K. This phase of the ISM is mostly observed in emission lines (like 21 cm line) but also slightly contributes to the spectrum by producing weak absorption features. There are difficulties with observations of the WNM absorptions features because of its low value of optical depth ($\tau_{\max} \sim 10^{-3}$) when compared with the CNM. This results in the fairly large uncertainty of the determined temperature values.

WNM fills around 50% of the volume of the Galactic disc (Heiles & Troland, 2003) and is thought to be in two forms – thermally stable form ($5000 - 8000$ K) and thermally unstable (below 5000 K) which will turn into a thermally stable form or it will cool and become CNM. According to the model proposed by McKee & Ostriker, the CNM is concentrated in the core of the clouds which is surrounded by warm neutral medium. Furthermore, Inoue & Inutsuka (2009) studied 2D magnetohydrodynamic simulations which have shown that WNM may be important in the process of formation of molecular clouds.

Both forms of the neutral medium also contain a small fraction of ions. Ionization of the material is mostly caused by cosmic rays. Hydrogen and helium in CNM clouds resist long wave radiation but high-energy photons (X-ray) can ionize atoms inside these clouds, if a source of such radiation is present. Results of modeling of such problem are strongly influenced by the presence of dust grains in the medium. Grains are also a source of photoelectrons which play an important role in the heating mechanics of the neutral medium.

3.2 Diffuse Molecular Gas

If the density of a given part of the ISM is high enough, its interior will be partially protected from outer ionization and dissociation sources by a diffuse atomic gas. This allows molecules to exist for extended periods of time. In such regions, most of the hydrogen is in the form of H_2. Many other important interstellar molecules are also present in this phase of ISM, such as carbon monoxide which is the second most abundant molecule. In

fact, it is CO that is usually used for tracing the molecular gas, as its radio emission can be relatively easily observed in comparison with strongest H_2 absorption lines in the UV part of the spectrum. However, this observational method cannot be used to probe outer parts of diffuse interstellar clouds where H2 can still be very abundant but the number of CO molecules will be lower because of the dissociation ($E_{\mathrm{dissCO}} = 3.7$ eV, $E_{\mathrm{diss}H_2} = 4.5$ eV).

Molecular hydrogen plays a very important role in processes which occur in the diffuse molecular gas. This mostly neutral medium contains a small amount of H_2^+ and free electron (fraction of ionized molecules $\sim 10^{-4}$). These ionized molecules then react with neutral molecules and change the chemical composition of the cloud. For example, the molecule H_3^+ is mostly formed due to the reaction

$$H_2^+ + H_2 \rightarrow H_3^+ + H\,. \tag{3.1}$$

It is the molecule H_3^+ that reacts with neutral atoms and other molecules to form some of the most important molecules, such as HD, OH, CH and HCO.

A significant amount of carbon in outer layers of molecular gas is ionized. Because of its high abundance and the fact that it is the source of most of the free electrons in these parts of the medium, the number density of C^+ is almost equal to the electron number density, with X-ray photons and cosmic rays being the main source of ionization. The discovery of the ionized carbon molecule (CH^+) was first reported by Herzberg & Douglas (1941). The abundance of CH^+ in molecular gas is higher than expected which has been known for decades but the process of its formation is still not completely understood. The most probable reaction

$$C^+ + H_2 \rightarrow CH^+ + H \tag{3.2}$$

is highly endothermic but the source of such amount of energy is presently unknown. Bacchus-Montabonel & Wiesenfeld (2013) investigated an alternative reaction

$$C_2^+ + H_2 \rightarrow CH^+ + H^+\,, \tag{3.3}$$

but results of their computation showed that such reaction is not very efficient.

By using the Heterodyne Instrument for the Far-Infrared (HIFI) of the Herschel Space Observatory gave us a significant amount of information about the ISM. Sonnertrucker et al. (2010) discussed the important role of hydrogenfluoride in observational astrophysics. It was shown that HF could be used as a tracer of molecular gas, as it was previously theorised, even in regions with low H_2 abundances.

It is generally thought that cosmic rays and dust grains (due to photoelectrons or perhaps H_2 formation) are the main heating source of molecular gas. On the other hand, CO line emission is most likely the main cooling mechanism. However, many unexplained observations show that our understanding of these processes in regions with molecular gas is still very limited.

3.3 Diffuse H II Gas

Temperatures and densities of the ISM are often similar to those in warm neutral medium with one important difference – the atomic hydrogen is usually found ionized. Also

called warm ionized medium (WIM), these regions of the ISM are mostly concentrated in the Galactic stellar disc and extend to about 1 kpc from the Galactic plane. Good examples of the WIM are the well known and easily observed objects called planetary nebulae (PNe). PNe are remnants of evolved stars of asymptotic giant branch with masses $1M_{\odot} < M < 8M_{\odot}$ that are ionized by the degenerate central stellar core. Radiation of this core drives the expansion of PNe to above 20 km/s. The strongest emission lines observed in their spectra are of H II and He II but forbidden lines of ionized and highly ionized oxygen and nitrogen are also present.

Possible ionization sources for diffuse H II gas were discussed by Reynolds (1984). Radiation from white dwarfs and supernova remnants seem to be important sources of photoionization but OB stars are most likely the main source, although results of some works do not support this idea. For example, Kwang-Il Seon (2009) attempted to model H_{α} emission of the galaxy M 51. It was found that Lyman continuum photons from dense H II regions could not explain the existence of diffuse ionized gas. On the other hand, there are works which support the hypothesis that OB associations are the source of ionization for ionized gas. Ferguson et al. (1996) studied large-scale distribution of this phase of the ISM. One of the results of their work is that there is a correlation between the diffuse H II gas and the H II regions. Moreover, this medium accounts for $30-50$ % of H_{α} emission of spiral galaxies. Their calculations also support the hypothesis that diffuse H II gas is ionized by photons escaping H II regions. Finally, the contribution of the diffuse gas to H_{α} emission seems to be almost the same in all observed spiral galaxies.

At first, low ionization levels were predicted for the WIM. However, observation of forbidden oxygen lines [O I] showed that these lines are very weak compared to those of highly ionized oxygen. Furthermore, Haffner et al. (1999) observed H_{α}, [S II] and [N II] towards Orion and Perseus arms and found that [S II] $\lambda 6716$ Å and [N II] $\lambda 6583$ Å anti-correlate with H_{α} which decreases with distance from the Galactic plane. On the other hand, [S II]/[N II] was found to be constant with varying H_{α} intensities but has different values in regions with different local ionization conditions.

3.4 Stellar Outflows

Most of the main sequence stars in our Galaxy are cool-type objects ($T_{\rm eff} < 7000$ K). A significant amount of these cool stars will evolve into stars of the asymptotic giant branch (AGB) with high mass loss rates. However, these stellar winds have low velocities which means that the density of such outflow is relatively high and makes this medium an unlikely source of DIBs. Moreover, studies of the circumstellar medium of post-AGB stars, e.g. Luna et. al (2007), show that carriers of the DIBs are most likely not present in their circumstellar envelopes.

Outflows from some hot stars are fast enough to have densities low enough to be called a "diffuse medium", but there seems to be no reason for DIBs to be formed there. However, the interaction of the stellar wind of hot stars with other forms of ISM may be important, as mentioned in Section 3.5.

3.5 Hot Ionized Medium

Spitzer (1956) was the first who presumed the existence of a Galactic corona. One of its first indicators was the presence of normal interstellar clouds as far away from the Galactic plane as 1 kpc. Spitzer pointed out that a typical cloud with a radius of 5 pc should expand in very low-density environment, achieving equilibrium in 10 million years. Because such clouds are observed, they have to move through a medium with the pressure similar to that in the Galactic plane where such clouds are usually observed. He proposed that a low-density gas at temperatures between 10^5 K and 10^6 K could explain the observations.

Hot ionized medium (HIM), often called coronal gas, is the hottest form of the ISM with temperatures above 100 000 K. This medium is generated by high-velocity stellar winds which collide with the surrounding gas that becomes shock-heated. Even more important is the role of novae and supernovae, where quickly expanding remnants of stellar atmospheres are driven by radiation pressure. These have velocities of about $10^3 - 10^4$ km/s.

The interaction of stellar outflows with HIM leads to high degree of ionization of many atoms in these regions of space. UV absorption lines of species, which have ionization potentials above 100 eV, are usually observed, since no other phase of the ISM has temperature high enough to produce such lines. However, this medium can also be observed in radio and X-ray emission, although radio synchrotron emission is usually only used to probe the medium surrounding galaxies.

There are several sources of the X-ray emission coming from the hot ionized medium and all of them serve as the cooling mechanism for the medium. Continuum free-free emission is caused by deceleration of a charged particle (usually an electron) in the presence of heavier charged particle (an atomic ion) – a such process is referred to as bremsstrahlung. X-ray emission lines are the result of collisional excitation due to the shock waves. Collisions may lead to recombination which is also a source of line emission.

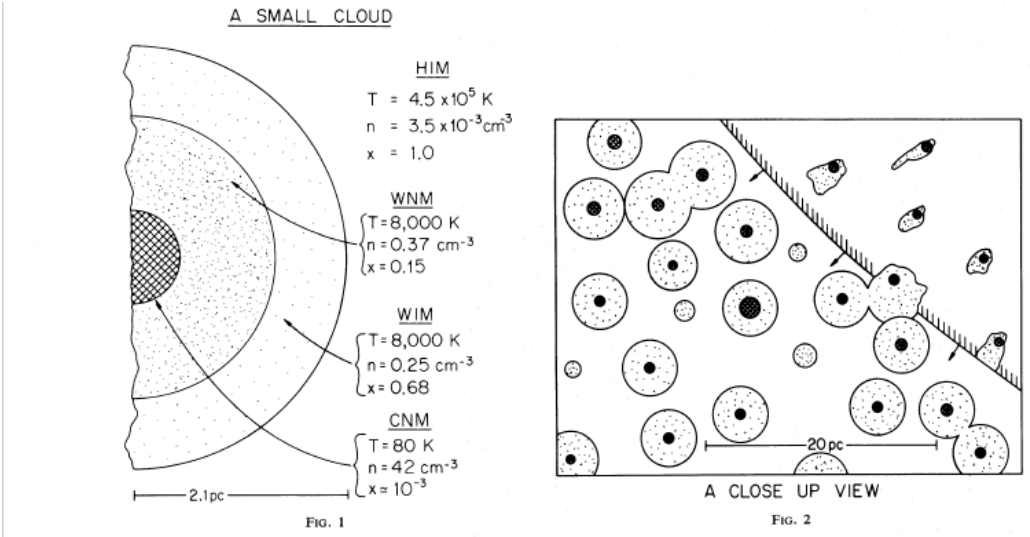

Figure 3.1: A simple illustration of the ISM containing clouds that are composed of a core and progressively hotter layers of gas. In this model, the HIM fills the space between the clouds. Taken from McKee & Ostriker (1977).

Tüllmann et. al (2008) investigated the HIM in the largest star-forming region, NGC 604, of the galaxy M 33. By studying the X-ray emission coming from this region, they found that NGC 604 is filled with bubbles and cavities which contain gas with temperature over 5 000 000 K. This indicates that the coronal gas is also present in galactic discs and occupies a large fraction of their volume. In fact, coronal gas fills most of the volume of our Galaxy and its density is therefore extremely low. It is also worth mentioning that HIM is very likely the form of baryonic matter which fills most of the voids between galaxies.

An example of a cavity filled with the coronal gas is the Local Bubble where our Solar System resides. It is the source of a small fraction of observed X-ray emission. Kuntz & Snowden (2008) obtained XMM-Newton spectrum of X-ray emission, studied the O VII line at 2.2 Å estimating $T \sim 1.2 \times 10^6$ K for the Local Bubble. Its origin was often studied and it appears that supernovae are the most likely candidates. Maíz-Apellániz (2001) used astrometric data and evolutionary models and predicted that about 20 supernovae occurred near the Solar System over the last 12 million years, of which six may have been responsible for the creation of the Local Bubble.

Chapter 4

Fullerene C_{60}

As it was mentioned before, one of the interesting properties of fullerenes is that they are quite resistant to fragmentation. This makes them the perfect candidates for the origin of the diffuse interstellar bands. While they have already been confirmed to be part of the ISM, their spectra are still very poorly explored.

Now, let us take a closer look at our understanding of the molecule C_{60} – one of the smaller fullerenes. The use of several approximations is required in order to build the spectroscopic model. So far, not much work has been done regarding this problem. A simple program is required for the calculation of the energy levels and it will also be used for matching the corresponding transitions with the DIBs at 9577 Å and 9632 Å.

4.1 Basic Information

Kroto et al. (1985) used the techniques of the mass spectrometry to analyse the structure of the C_{60}. It is assumed that the molecule resembles a truncated icosahedron which has 12 pentagonal faces, 20 hexagonal faces and 60 vertices which lie on a common sphere. Its shape is very similar to that of a football.

Even more important, its symmetry (e.g. discussed by Konstant, 1994) leads to the reduction of possible vibrational modes. Experimentally, 46 different modes were observed and only 4 of them are active in the infrared part of the spectrum. Furthermore, restrictions to the occupation of rotational states based on the boson-exchange symmetry were discussed by Sogoshi et al. (2000). In combination with the known vibrational modes, the research team was able to simulate the gas phase spectral bands of the C_{60} – unfortunately, their model failed when it was compared with laboratory observations (Figure 4.1). The team also published the spectrum of the molecule. In Figure 4.2 we can see the observed absorption spectrum ($5200 - 6400$ Å region) of a C_{60}/pH_2 solid. Interesting enough, we can easily identify strong absorption features at 5800 Å and 5900 Å where several DIBs are also located.

Since its discovery, the buckminsterfullerene was thought to be present in the ISM as a relatively common molecule. Kroto et al. (1987) studied the connection between grains and carbon chain molecules. Kroto pointed out that the vaporization of graphite can lead to the elevation of the number of molecules, such as C_3, C_7, or C_{60}. Grains with high content of carbon are usually associated with the circumstellar medium of the carbon stars. Moreover,

as long chains of molecules condensate in the presence of both, hydrogen and nitrogen, cyanopolyynes are produced. A possible proof of their presence can be found by observing spectra of carbon-rich stars (e.g. CW Leonis). Evidence seems to point to the possibility of carbon stars being the source of the mentioned molecules but this has not been confirmed yet. Finally, a very crucial laboratory experiment was done by Foing & Ehrenfreund (1994) who measured infrared spectra of ion C_{60}^{+} trapped in a neon matrix. They found that two bands which are located near 9577 Å and 9632 Å, where two of the observed DIBs are located as well.

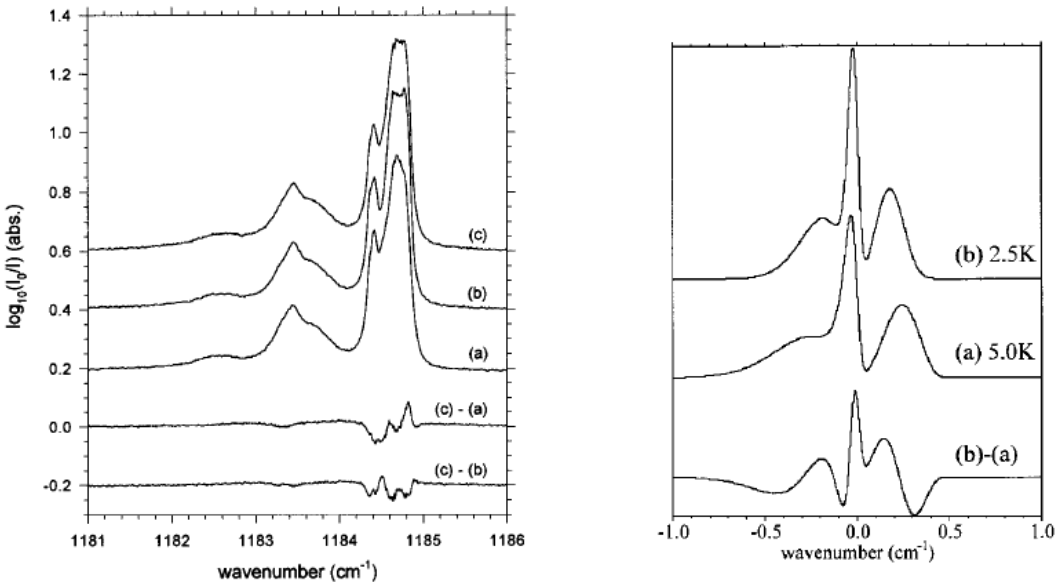

Figure 4.1: Comparison of the observed laboratory (left) spectrum with theoretical prediction (right) of the $T_{1u}(3)$ vibrational mode of C_{60} at different temperatures.

In the past ten years, several observations were made which unambiguously confirmed the presence of fullerenes in the ISM. Cami et al. (2010) studied the spectrum of the planetary nebula Tc 1 and found features which resemble vibrational bands of C_{60} and C_{70}. Berné et al. (2012) also examined the infrared spectra of a reflection nebula. NGC 7023 and its surrounding environment were found to contain neutral C_{60} and PAHs. The detection of 4 more (unknown) bands was also reported – the team associated these features with laboratory spectra of the ion C_{60}^{+}. Otsuka et al. (2013) used this knowledge and searched data archives for spectra of PNe that contain 17.4 μm and 18.9 μm features which appear due to the presence of buckminsterfullerene in the observed medium. They reported six new detections of the fullerene in planetary nebulae (eleven in total) and also found that most of these PNe are located further from the Galactic centre than the Sun.

4.2 Formation and Location of C_{60}

Up until 2010, fullerenes were considered to form in medium with relatively low abundance of hydrogen as was pointed out by theoretical and experimental works, for example by Jäger

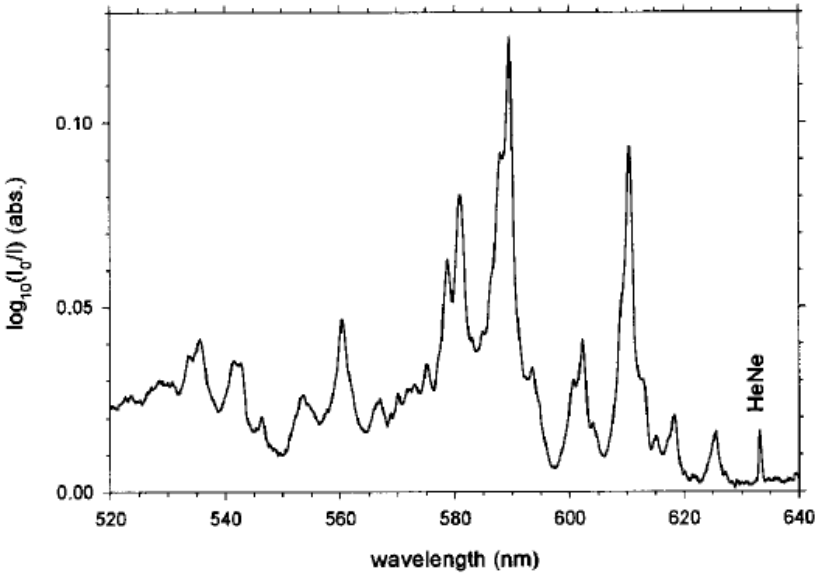

Figure 4.2: Absorption spectrum of the C_{60}/H_2 solid.

et al. (2009) and Kroto et al. (1985). This was challenged by the work of García-Hernández et al. (2010) who detected both, PAHs and fullerenes in hydrogen-containing PNe observed within our Galaxy and the Small Magellanic Cloud. They suggested that these complex molecules may be formed as a result of the destruction of hydrogenated amorphous carbon (small dust grains).

García-Hernández et al. (2011) studied more PNe in the Magellanic Clouds and came up with three very important results. Firstly, they reported the first detection of C_{70} outside of our Galaxy. More importantly, they observed fullerene emission towards stars with effective temperatures $T_{\rm eff} < 25\,000$ K which could not be explained by a molecule contained on the surface of dust grains. Instead, a possible explanation was proposed – C_{60} molecules are in the gas phase and are excited by UV radiation. Finally, the team noticed different ratios of intensities of forbidden lines [Ne III]/[Ne II] (this ratio indicates the strength of the radiation fields) which cannot be explained by the photoionization alone. Together with the detection of P-Cygni profiles in the UV region, this seems to suggest that shocks driven by stellar wind ($v > 1000$ km/s) may be the cause of the destruction of small grains which leads to the formation of fullerenes.

Although it is usually thought that the C_{60} is formed in envelopes of stars, Berné & Tielsen (2012) analysed data from Herschel and Spitzer and found that this molecule may also be formed efficiently in interstellar clouds if a source of UV radiation is present. An alternative way of formation of the studied fullerene was presented – some PAH molecules may be converted to graphene which after the loss of a single carbon atom may form into the C_{60}. A similar approach was examined by Zhen et al. (2014). Briefly, their experimental method consists of analyzing photo-fragmentation of PAH cations $C_{60}H_{22}^+$, $C_{66}H_{26}^+$ and $C_{78}H_{26}^+$ (which should be most stable in the interstellar environment) and of fullerenes C_{60} and C_{70}. This study showed that PAHs containing more than 60 carbon atoms can be photo-isomerized to the C_{60} fullerene. This process occurs when light interacts with molecules and causes excitation – this may lead to the unpairing of bonding electrons. At

this state, these electrons tend to pair up in such way that a new isomer of the molecules is formed.

These works give us a vague idea about the conditions required for fullerenes to form in space. However, when we observe them in the ISM, their location may not coincide with the place of their birth. In order to find what phase of the medium they belong to, one must use good tracers of these environments.

First of all, tracing the coronal gas may be very difficult in this study since the features that are usually associated with it are located in far-UV and X-ray regions. On the other hand, molecular gas can be easily observed thanks to the CO lines. A relation was found and it leads to the statement that if carbon monoxide exists in the medium, dust grains must be present as well. This is because of the fact that grains are able to shield molecules from the high-energy radiation that would otherwise destroy their bonds. Studying CNM and WNM can be very difficult as their best tracer is the neutral hydrogen. The problem is that hydrogen lines are usually also present in the atmospheres of the observed stars. Therefore, interstellar H I will not be usually seen in the lines of sight towards such objects. Other interstellar species can also be used to probe the warm neutral medium but they are not as reliable as hydrogen. For example, Welsh et al. (2009) tried to construct maps of Na I and Ca II interstellar absorption. They also examined the idea that these atoms might be useful for studying the interstellar medium at temperatures lower than 10 000 K. Since calcium is expected to be captured by grains in dense molecular clouds, the ratio Na I/Ca II tends to be quite high (> 100). A low value of this ratio can be the consequence of two possibilities – the Na and Ca are part of the warm partly ionized medium (WNM) or the medium where they are located must be shock-ionized. Unfortunately, it is uncertain whether this technique also traces the diffuse H II gas. However, there are some lines that can be used in the case of novae and remnants of supernovae, for example [Ne III] and [O III].

It is possible to find the origin of C_{60} bands in the ISM by measuring the variation of the strength of the lines of the mentioned tracers in different directions. However, it is also very likely that no correlation will be found because of a different relation between the given spectral feature and the host environment.

4.3 Association with DIBs

Campbell et al. (2015) were able to make precise laboratory measurements and showed that the NIR gas-phase spectrum of C_{60}^+ embedded in a neon matrix and cooled down to low temperature, coincides with two DIBs located at 9577 Å and 9632 Å. The work gives the most probable association of a molecule to DIBs to this date. They discussed that the transitions that produced these features should originate from the lowest vibrational level of the ground electronic state. Electronic transitions of ionized buckminsterfullerene were studied by Fulara et al. (1993), for example.

It was argued that not only the laboratory bands lie very close to the two DIBs, but they are also very narrow (full width at half maximum ~ 2 Å). The translational temperature of C_{60}^+-He stored in cold helium was estimated to be ~ 150 K. This could point to the fact that diffuse molecular clouds have temperatures of the same order but it should also be carefully considered whether the large fraction of the C_{60} would be ionized under such conditions. The ionization energy of neutral C_{60} is ~ 7.6 eV (Pogulay et al., 2004) while

the dissociation energy of the carbon monoxide, which is used as a tracer of molecular clouds, is about 11.1 eV. It is reasonable to expect that if a source of ionization, for example a hot star, is present in such medium, a large number of the C_{60} molecules could indeed be ionized.

Additional proof of the C_{60}^{+} ion being responsible for DIBs was found by Walker et al. (2015). They analysed the spectrum of HD 183143 (one of the commonly observed stars when dealing with DIBs) and found that at least one other band reported by Campbell et al. was found in the spectrum.

It appears that we have finally revealed the first carrier of the DIBs, after almost one hundred years. However, additional information is still required – if C_{60} is truly responsible for these two (or three) bands, several more bands should also be present in observed spectra. Proper identification can be difficult because the $9000 - 10\,000$ Å region is obscured by telluric lines. Therefore, the results of Campbell's work have to be theoretically recalculated which might lead to the discovery of more, perhaps weaker features associated with this molecule.

4.4 Chosen Model of the Molecule

The complexity of the structure of the C_{60} makes it impossible to properly calculate its eigenstates. Therefore, we have chosen to work with several approximations which will be discussed in this chapter.

The easiest way of dealing with electronic transitions is to find those that have already been observed in laboratory experiments. Specifically, we are working with the cation C_{60}^{+} which has transitions different from the neutral molecule. Fulara et al. (1993) were able to find several electronic transitions of, both, C_{60}^{+} and C_{60}^{-} in the IR part of the spectrum where the 9577 Å and 9632 Å DIBs are located. In the case of the cation, bands were present at wavelengths between 10368 Å and 10435 Å. These results will be used for the determination of the possibility of 9577 Å and 9632 Å bands originating from these transitions.

I have used the spherical symmetry of the molecule for creating a simple rovibrational model. A very good approximation is having the molecule rotate as a sphere with a rotational constant ~ 0.0028 cm^{-1} (Edward & Leach, 1993) – the precise value depends on the vibrational mode and on the presence of isotopes. Its vibrations are described by inflation/deflation of a sphere with frequencies corresponding to the oscillations of a real C_{60} molecule. We have used the values from Jing & Pan (2009) who mentioned results of other works but we have also applied another useful work regarding C_{60} vibrations (Parker et al., 2011). The lowest energy needed for the dissociation of the C_{60} is about 10.0 eV and corresponds to the removal of C_2 from C_{60}^{+}.

The calculation of rovibrational lines is therefore relatively straightforward – we have taken the equation 2.35 and used it for finding the corresponding energy levels. However, the usefulness of this model strongly depends on the vibrational mode it is working with. Most of the modes are not well represented by simple radial oscillations but they are more appropriately described by other complicated deformations of the sphere. Therefore, this model is suitable only for the vibrational mode designated as $A_g(1)$ (work by Menéndez & Page, 2000) and has only very limited use for other modes.

4.5 Calculated Energy Levels

The first model that can be tested is the harmonic oscillator. When we tried individual oscillator frequencies from the literature (Jing & Pan, 2009), only transitions between high vibrational quantum numbers ($n \sim 70 - 80$) produced lines at 9577 Å and 9632 Å. These results are extremely unlikely, since very high energy source (radiation or temperature) would be required, but this would result in the destruction of the molecule.

More probable values are found by using the Morse potential. In the articles cited above, the possibility of the two bands resulting from electronic transitions was mentioned. Therefore, calculations of rovibrational energy levels shifted due to the presence of electronic term are also performed.

4.5.1 Boltzmann Distribution – Populated States

It is necessary to estimate the temperature of the medium and find the most occupied rotational and vibrational states before calculating energy levels. We have used the equation for rovibrational energies 2.35 for a Boltzmann distribution in which the temperature plays a role of a free parameter. In the procedure described below, the distribution of rotational levels has been found by using a fixed vibrational state, and vice versa. All other parameters in the equation must be known before working with the Boltzmann distribution.

For the C_{60} molecule, the temperature can range from very low values (for example, 150 K from Campbell et al., 2015) up to the high values at which the molecule would dissociate. This was studied by Openov & Podlivaev (2006) and they found that the molecule starts to change its structure and breaks at temperatures between 4000 K and 6000 K – this would give the highest amount of highly populated levels. It can be calculated for the case of separate vibrational and rotational levels that the most occupied states are $n_{\mathrm{fix}} = 0$ and $700 < J_{\mathrm{fix}} < 865$. These numbers have been used as the fixed values in the rovibrational case and found the rotational distributions at 145 K and 5000 K (Figure 4.3). We will refer to these values as the low-temperature and high-temperature case, respectively.

4.5.2 Purely Rovibrational Transitions

At first, we only worked with the assumption that 9577 Å and 9632 Å bands are due to the C_{60} molecule. Based on this, only two unknown parameters remain in the equation 2.35 – the vibrational quantum numbers of the two states corresponding to the transition. However, these numbers are integers and they should have low values. Therefore, we have chosen to take the oscillator frequency as the unknown parameter and test various quantum numbers that fit both transitions (9577 Å and 9632 Å) for a given parameter value. This gives an infinite number of solutions but only a few of them are physically meaningful.

I required the tested vibration parameters to fall within the range $200 - 1600$ cm^{-1} that corresponds with the laboratory values. The whole process of seeking this parameter was done semi-automatically by a custom program. This program takes several constants into account (rotational quantum numbers, rotational constant and dissociation energy) and requires an input in the form of two vibrational numbers n_1 and n_2. The procedure we have written then uses the known wavelength of the resulting transition and gives

the frequency of the vibrational mode in the output. In the case that calculated values fall within the mentioned range, another condition will check whether the second line can also be produced by reasonably low vibrational numbers n'_1 and n'_2. Furthermore, the Boltzmann distribution must predict that such states can be populated enough – this is constrained only by the kinetic temperature of the gas.

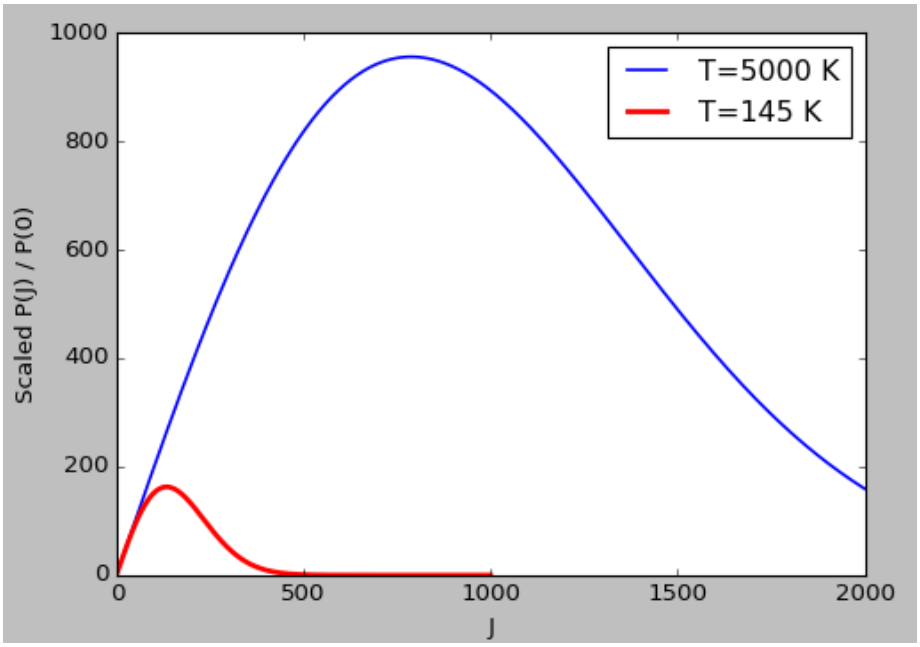

Figure 4.3: Population of the rotational levels at 145 K and 5000 K.

This approach leads to several possible results. In order to pick the most likely ones, we have searched for other predicted lines in observed spectra of stars taken by the X-Shooter spectrograph which will be further discussed in Chapter 5. The more lines with narrow profiles are found near the positions calculated by the program, the higher is the probability that the model using the given oscillator frequency is satisfactory. To be sure, we also had to check whether these lines are not originating from known interstellar or telluric carriers. we have taken models calculated using ESO's SkyCalc tool, which are described by Noll et al. (2012) and Jones et al. (2013), as reference telluric spectra.

Out of all values we tried, the best result was found using the following assumptions:

ν [cm^{-1}]	J_2	J_1	n_2	n_1
932.033	1400	1370	12	0

with overall 29 lines found in different spectra. Of those, 22 were present in most of the examined X-Shooter data and are listed in the table below. When comparing with tables of telluric lines, we have found that only 3 of the observed lines can be associated with an interstellar carrier. Further investigation of these features will be done in the next chapter.

Table 4.1: List of the C_{60} vibrational lines calculated with $\nu = 932.033$ cm^{-1}. Features observed in stellar spectra that have comparable wavelengths are labelled as associated.

Transition	$\lambda_{\text{calculated}}$ [Å]	$\lambda_{\text{associated}}$ [Å]	Comment
$7 \rightarrow 2$	22803.6	22802.2	telluric
$6 \rightarrow 1$	22668.2	22667.6	telluric
$5 \rightarrow 0$	22534.4	22534.0	telluric
$7 \rightarrow 1$	18942.4	18942.8	telluric
$9 \rightarrow 2$	16378.2	16372.2	-
$8 \rightarrow 1$	16281.7	16282.6	possibly telluric
$9 \rightarrow 1$	14286.6	14285.9	telluric
$10 \rightarrow 1$	12735.1	12734.2	telluric
$9 \rightarrow 0$	12660.7	12661.7	telluric
$13 \rightarrow 3$	11630.9	11620.1	telluric
$12 \rightarrow 2$	11562.2	11562.0	telluric
$11 \rightarrow 1$	11494.2	11494.8	telluric
$10 \rightarrow 0$	11427.0	11425.8	telluric
$14 \rightarrow 2$	9690.5	9692.0	-
$13 \rightarrow 1$	9633.4	9633.4	blend
$12 \rightarrow 0$	9577.0	9577.0	telluric
$15 \rightarrow 2$	8970.9	8969.1	weak
$16 \rightarrow 2$	8354.2	8353.6	weak
$15 \rightarrow 1$	8304.9	8305.1	-
$14 \rightarrow 0$	8256.1	8256.5	possibly telluric
$17 \rightarrow 1$	7309.0	7309.6	telluric
$16 \rightarrow 0$	7266.0	7265.6	telluric

I have also recalculated the energy levels in a more traditional way, by using the laboratory measured oscillator frequencies from Parker et al. (2011). The lowest oscillator frequency that was able to produce a reasonable ($n_2 < 15$) transition below 10 000 Å was 774.5 cm^{-1}. However, none of the modes was able to produce lines near 9577 Å and 9632 Å while using reasonable values of J and n, except of the 945.6 cm^{-1} A_u mode. This is to be expected, since the frequency is very similar to the value calculated above. Unfortunately, this mode does not produce radial oscillations and therefore, the model most likely does not describe the molecule well. The purely radial oscillation of the C_{60} molecule ($\nu = 497.2$ cm^{-1}) was able to produce first transitions below 10 000 Å when the vibrational quantum number reaches the value $n_2 = 22$. This state starts to be significantly populated $\left(\frac{P(n=22)}{P(n=0)} = 0.07175\right)$ at temperatures around 6000 K, as well as many other states. It follows that high amount of transitions, even if many of them were not allowed, would be located in the NIR part of the spectrum but this has not been found, yet.

The highest observed C_{60} oscillator frequency is 1571.1 cm^{-1}. We have listed all NIR transitions with $n < 10$, $J_2 = 760$ and $J_1 = 740$ in the table below. This gives relatively good results which should be checked in the spectra. However, the uncertainty area ~ 50 Å around the predicted wavelengths is very large and the NIR region is populated with

many lines. Therefore, we have chosen to use the known possibly identified DIBs between 10 000 Å and 18 000 Å by Cox et al. (2014). Based on this, only a match of 13 175 Å DIB corresponding to 13 211.2 Å calculated transition can be made. Unfortunately, this match is very uncertain and together with the lack of other matches, it makes this model inapplicable.

Table 4.2: Calculated vibrational transitions with oscillator frequency $\nu = 1571.1$ cm^{-1} and $n < 10$.

Transition	$\lambda_{\text{calculated}}$ [Å]	Transition	$\lambda_{\text{calculated}}$ [Å]	Transition	$\lambda_{\text{calculated}}$ [Å]
$3 \rightarrow 0$	21815.0	$7 \rightarrow 0$	9525.6	$8 \rightarrow 5$	22896.4
$4 \rightarrow 0$	16437.2	$7 \rightarrow 1$	11167.0	$9 \rightarrow 0$	7479.5
$4 \rightarrow 1$	22023.0	$7 \rightarrow 2$	13466.1	$9 \rightarrow 1$	8455.3
$5 \rightarrow 0$	13211.2	$7 \rightarrow 3$	16916.7	$9 \rightarrow 2$	9710.7
$5 \rightarrow 1$	16594.0	$7 \rightarrow 4$	22671.6	$9 \rightarrow 3$	11385.3
$5 \rightarrow 2$	22235.1	$8 \rightarrow 0$	8374.5	$9 \rightarrow 4$	13731.1
$6 \rightarrow 0$	11061.0	$8 \rightarrow 1$	9617.3	$9 \rightarrow 5$	17252.2
$6 \rightarrow 1$	13337.4	$8 \rightarrow 2$	11275.1	$9 \rightarrow 6$	23125.6
$6 \rightarrow 2$	16753.8	$8 \rightarrow 3$	13597.3	–	–
$6 \rightarrow 3$	22451.2	$8 \rightarrow 4$	17082.8	–	–

4.5.3 Electronic Transitions

In the next step, we recalculated rovibrational transitions with small adjustment – we added electronic shift T_e to the equation. Unlike in the previous case where we mostly considered very high temperatures, this time we have also used the lower values of the temperature ($T < 1000$ K) at which only the lowest vibrational states are considerably populated. There are two unknown parameters – the vibrational mode and the electronic shift. Fortunately, we were able to work with two of the DIBs which, in theory, simplifies the problem to two unknown values with two different equations.

If the temperature of the medium is high, many solutions can be found. Three of those, which have noticeably different parameters, are shown in Table 4.3.

Table 4.3: Electronic transitions, producing lines at 9577 Å and 9632 Å, calculated using three different combinations of the two parameters.

ν [cm^{-1}]	T_e [cm^{-1}]	Transition	λ9577 [Å]	Transition	λ9632 [Å]
1000	8500	$6 \rightarrow 4$	9579.9	$11 \rightarrow 9$	9633.0
1182	9280	$3 \rightarrow 2$	9578.5	$10 \rightarrow 9$	9630.4
1470	9000	$2 \rightarrow 1$	9572.0	$7 \rightarrow 6$	9629.3

It should be noted here that the first result ($\nu = 1000$ cm^{-1}, $T_e = 8500$ cm^{-1}) looks a bit similar to the case without the electronic shift (Table 4.1, transitions $12 \to 0$ and $13 \to 1$). The difference lies in the transitions themselves – $\Delta n = 2$ is much more likely to occur than $\Delta n = 12$. These results should be compared with observed spectra to verify such model.

On the other hand, if the medium, where the C_{60} resides, has a low temperature, only states up to about $n = 3$ are populated. We were unable to find any reasonable combination of the unknown parameters that could produce both of the DIBs.

4.5.4 Two Distinct Electronic Shifts

Finally, we have also explored the possibility of the DIBs being caused by the change of rovibrational state with two different electronic shifts. In this case, the second electronic shift becomes the second unknown parameter while we consider the vibrational mode to be known (1419 cm^{-1} $H_g(7)$ mode produces best matches). Fulara et al. (1993) found two very close electronic transitions at 10 368 cm^{-1} and 10 435 cm^{-1} (in the neon matrix). Although they might be the product of the interaction of C_{60} with the matrix it was embedded in, it is worth investigating whether such transitions may be the cause of the DIBs in 9000 Å region.

The best result, that we were able to find, used electronic shifts 9044 cm^{-1} and 8984 cm^{-1} ($\Delta T_e = 60$ cm^{-1} comparable with $\Delta T_{e,\,\mathrm{Neon}} = 67$ cm^{-1}) and fixed rotational quantum numbers $J_2 = 140$ and $J_1 = 137$ that correspond to the most populated levels at the temperature $T \approx 145$ K. In both cases, vibrational states change from $n = 1$ to $n = 0$. The calculated transitions seem to be reliable and can be readily compared with the work from Campbell et al. (2015) and observed spectra.

4.6 Isotope Effect – C_{60}

The presence of an isotope in a molecule can significantly change its rovibrational spectrum. The more of carbon atoms a fullerene has, the higher the probability of two isotopes of molecules being present in the medium is. This can be used for tracing large molecules.

This problem was discussed in several works – we have worked with the summary presented by Sogoshi et al. (2000). It appears that the presence of the ^{13}C causes the vibrational modes to split – in the case that one ^{13}C is present, the shifts are $\sim 0.5 - 2.0$ cm^{-1} from the original modes. The probability P_{iso} that a C_{60} contains N isotopes ^{13}C depends on the number of ^{13}C and on the relative abundance of this isotope in the studied medium and can be calculated from the Bernoulli Trials formula

$$P_{\mathrm{iso}} = \frac{60!}{N!(60-N)!}\, p^{-N} \left(1 - p^{-1}\right)^{60-N}, \tag{4.1}$$

where $p^{-1} = {}^{12}C/{}^{13}C$. However, the abundance of ^{13}C varies between different places of the interstellar medium. For example, Langer & Lenzias (1993) observed spectra of carbon monoxide towards interstellar clouds which lie within the radius of 500 pc around the Sun. They found that the value of the ratio of p in the local ISM is between 57 and 74. Furthermore, they also found in their previous work (Langer & Lenzias, 1993) that the relative

abundance of ^{13}C isotope is $p \sim 30$ at 5 kpc from the Galactic Centre and this value rises with the galactocentric radius. Moreover, different types of the medium that can be found in the universe have different abundances of isotopes. For instance, Goto et al. (2003) observed higher ratios of carbon isotopes in the nearby molecular clouds (> 100) than in the local ISM (~ 60). Finally, Zinner et al. (2006) discussed the varying values of isotope ratios when dealing with different dust grains in the envelopes of AGB stars.

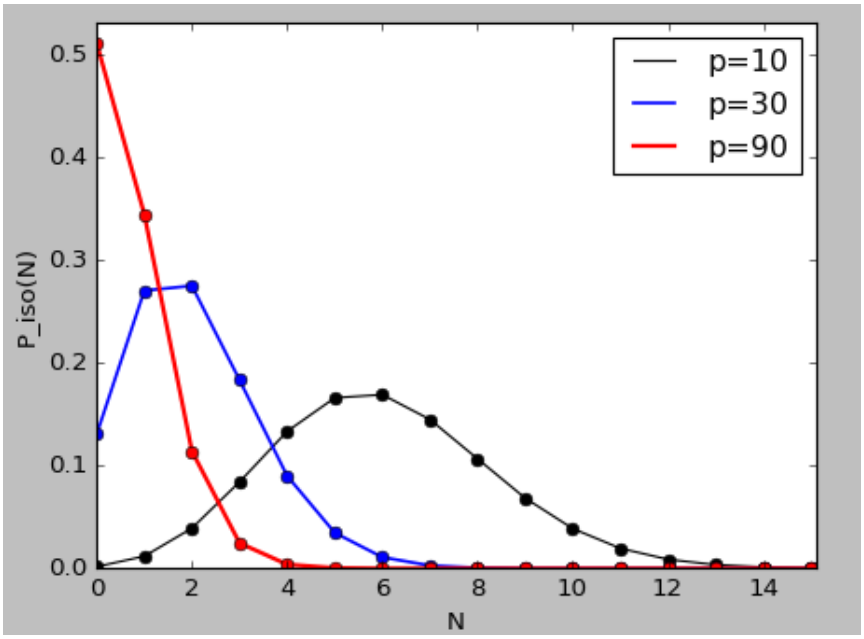

Figure 4.4: Probability of C_{60} containing N atoms ^{13}C in regions with different isotope ratios of carbon.

Let us test some of the ratios mentioned above and find the distributions $P(N)$. For simplicity, we have chosen six equidistant values 10, 30, 50, 70, 90, 110 and 130. The results can be seen in Figure 4.4 with maxima of distributions at $N = 6$ for $p = 10$, $N = 2$ for $p = 30$, $N = 1$ for $p = 50$, and $N = 0$ for $p \geq 70$. This means that we will find more $^{13}C^{12}C_{59}$ than $^{12}C_{60}$ for $p < 50$. More importantly, in the case of molecular clouds in Solar Neighbourhood where the value of p is high, we will have $\sim 30\%$ of the C_{60} molecules containing at least one isotope ^{13}C.

Obviously, the isotope effect is going to be spectroscopically very important when working with the molecule C_{60}. If this molecule is responsible for the bands at 9577 Å and 9632 Å, shifted bands should also be present. We have used the results from previous calculations of rovibrational bands and shifted the vibrational modes by 1 cm^{-1}. In the case of purely rovibrational transitions, there is a shift from 932 cm^{-1} to 931 cm^{-1} which results into DIBs shifting by about 10 Å to wavelengths 9586.9 Å and 9643.3 Å. In the case of the common electronic transition, the shifts (e.g., 9633.0 Å $\rightarrow$ 9634.7 Å, 9579.9 Å $\rightarrow$ 9581.7 Å) are much smaller but still possibly observable (full width at half maximum of the two DIBs is ~ 2 Å). Finally, in the case of the third calculation with two distinct electronic shifts, isotope effect is even smaller – bands are redshifted by 1 Å.

Searching for this effect in observed spectra is extremely important. It will not only tell us which model describes the molecule more accurately, it may also serve as an additional

proof that the C_{60} is really the carrier of the two diffuse interstellar bands. Moreover, isotope ratio, which would tell us more about the place of origin of the molecule, can also be derived.

Chapter 5

Stellar Spectra

It is necessary to be aware of several complications when dealing with spectra of stars. First, many publicly accessible data are the result of ground-based observations which means that the spectra are contaminated by telluric lines. It often happens that some of them are blended with interstellar features we are interested in, therefore they need to be removed. Another problem is that the NIR region, where all of the calculated lines are located, is densely covered with absorption features – this is especially true in the case of cool and evolved stars. Finally, DIBs have been only detected in the lines of sight towards reddened hot stars. Of course, the list of obstacles goes on, but it is clear that even the most basic thing – searching for the known DIBs, for example – can prove to be challenging. In order to avoid problems with complicated IR spectra, we have put a constraint on the stars whose spectra will be investigated by choosing only those with spectral classifications O and B.

Once detected, the spectral lines/bands have to be compared. A comprehensive way of doing this is calculating the so-called equivalent widths (EWs) of these features which represent the measure of their strength. Plotting the EWs from corresponding lines of sight then can be used to find correlations between the two plotted spectral lines. This is done for the two DIBs and associated lines, as well as for the known interstellar features.

5.1 The X-Shooter Spectral Library

The X-Shooter spectrograph is part of the Very Large Telescope (VLT). It produces medium resolution spectra ($R \sim 4000 - 17000$) that can be observed in three spectral regions: UVB ($3000 - 5595$ Å), VIS ($5595 - 10240$ Å), and NIR ($10240 - 24800$ Å). This is done by splitting the incident light into three parts which are then registered at three separate spectrographs. The data are in the form of FITS files which carry the information about wavelength, flux, flux error, reduced flux, reduced flux error and signal to noise ratio. The technical details are discussed by Vernet et al. (2011).

Spectra of a total of 92 O-type and 419 B-type stars have been chosen for the purpose of this work. The median signal to noise ratio varies from file to file – data which have S/N below 150 were filtered out by the program that calculates equivalent widths. Moreover, at least three files containing NIR spectrum do not contain data all the way to the 24 800 Å and they needed to be filtered out.

5.2 Removing Telluric Features

The absorption and scattering of the light in the atmosphere is mostly caused by H_2O, O_2, O_3 and several other molecules and limits the number of transmitted photons. It is mainly H_2O that causes most of the absorption in the visible and infrared parts of the spectrum. Moreover, some of the light might be scattered from other sources (Moon, other stars, zodiacal light, and so on) into the line of sight of the observed object. Both, this night-sky radiance and the transmission must be accounted for before working with spectra.

When taking into account a line of sight towards one star, for example, the amount of transmission and radiance changes throughout the observation. This is caused by the fact that the atmosphere is not stationary and conditions within it change in time. Furthermore, as the Earth rotates, the elevation angle above the horizon of the star changes. In the zenith, the effect of the atmosphere will be weakest – let us denote the radial thickness of the atmosphere as D. From the point of view of an observer, the thickness in the given line of sight has greater values as the elevation angle gets smaller.

The removal of the effects of the atmosphere can be done in two ways. First, a standard star can be observed simultaneously with the target. Spectral features of such standard stars are very well known and can be used to find the telluric lines. If we assume that the conditions in the atmosphere in the line of sight towards the standard star are the same as towards the second star, we can use the results to remove telluric lines from both objects. Unfortunately, as it was discussed above, this is only a first approximation, which is hardly fulfilled, and such process would not remove telluric features properly. A second option is to use models of Earth's atmosphere and predict the telluric lines in a given line of sight.

The atmospherical model we worked with is discussed by Noll et al. (2013). We used the ESO's SkyCalc tool to calculate the telluric lines for one of the stars. The standard approach is to make a wavelength-dependent shift of any one of the two spectra, because of the heliocentric velocity correction, so that the corresponding wavelengths of the atmospheric features match the ones seen towards the star. Then one has to either normalize the stellar spectrum or scale the modelled spectrum. The problem with the scaling is that the continuum of the atmosphere, at the time of the observation, is not given in advance. However, the continuum can be estimated by looking at some of the clearly defined features that are present in both of the spectra. If they are close to each other, their continuum flux should be almost identical. By taking the difference between peak and continuum fluxes in theoretical data, and estimating the peak fluxes for the same features in the observed data, we can easily find the unknown continuum. For the two features, it is directly given by solving a simple equation

$$\frac{F_{\mathrm{cont,mod}} - F_{1,\mathrm{mod}}}{F_{\mathrm{cont,mod}} - F_{2,\mathrm{mod}}} = \frac{F_{\mathrm{cont},*} - F_{1,*}}{F_{\mathrm{cont},*} - F_{2,*}}, \tag{5.1}$$

where F is the flux, the first index indicates the continuum or one of the two features, and the second index marks the data set (asterisk for the star, mod for the atmospheric model). Now, all values required for the scaling of the modelled spectrum are known. Once the spectra can be matched, we should be able to remove the telluric contamination by dividing the fluxes at corresponding wavelengths. Here, a problem arises, since the shift from the first step caused that the data points to be misaligned. To deal with this, we are

using linear interpolation to add points at the given wavelengths.

I have tested the procedure describe above on several stars but the program was unable to properly remove the telluric features.

5.3 Calculation of the Equivalent Widths

In principle, the calculation of equivalent widths of spectral lines is fairly straightforward. One only has to find the continuum at the position of the investigated line, the wavelengths at which it ends, and its peak absorption/emission. After that, the line has to be normalized which is done with the use of the continuum. Finally, simple integration between the two limiting wavelengths gives the area of the line below continuum. The equivalent width of the feature is found by dividing the area by the peak absorption/emission.

When working with real spectra, one will realise that this will require a bit more complex method to solve this problem. The results are mainly limited by the precision of locating continuum. However, the spectra are covered by noise which is in the case of many X-Shooter data files quite significant. Furthermore, other spectral features may also be present near the investigated line. In order to find the continuum at the position of a given line, we have developed a procedure that must be used before the calculation of the equivalent widths. We have decided to deal only with the small area around the line where the continuum can be well described by a linear function. The problem is to find the two points that would define such function. The range of x-values is $\lambda_{\text{line}} \pm \varepsilon$. By analyzing the region around all different lines with which the program will be working, we have found that epsilon can take values between $0.2 - 8.0$ nm in order to reach the best performance in the procedures described below. To illustrate this, $\varepsilon = 0.3$ nm is a good value when dealing with the sodium D-lines. However, lines in the IR region are rarely so narrow and well-defined as the Na I lines and the use of wider regions is required for finding the continuum.

The process of searching for the continuum is based on a statistical approach. It attempts to locate the two defining points by going through several data points and checking the mean value and standard deviation of y-values. If the deviation is small enough, the procedure has found the continuum and places a point at the mean value. On the other hand, if it is large then the next number of points is taken and conditions are checked again. This is done iteratively until the point where either the continuum has been found or the program has reached the end of the data array. If the second possible outcome occurs, the mean value of the first and second half of the array is taken – this is a very imprecise alternative way of finding the continuum at the line's position but it is used only very scarcely. This calculation is done for both, the left and the right side of the line. Unfortunately, it may fail on several occasions which should be mentioned. First, the limitation of the standard deviation changes from file to file, but only fixed values have been used instead. A possible improvement is trying several more reference values if the lowest one reaches fail condition. Furthermore, only lines which are clearly resolved in the spectrum can be used. The presence of many other features in the near vicinity of the line also leads to the alternative approach of evaluating continuum points.

Once the continuum is known, the program has to find the blue and the red end of the line itself. We tried two possibilities. The first one is based on calculating the differences

between y-values while starting from the approximate centre of the line. For example, the procedure is attempting to find the right end of the line with $x_2 > x_1$. If $y_2 > y_1$ than the difference is a positive number and the end of the line has not yet been reached – this happens only when $y_2 \leq y_1$. To account for noise, this conditions have to be checked for $y_1 = y_i$ and several subsequent y-values $y_1 = y_i$, $y_2 = y_{i+1}$, $y_2 = y_{i+2}$ and $y_2 = y_{i+3}$. If the condition is not met, the procedure skips these points and moves to $y_1 = y_{i+3}$, and so on. This process tends to work very well but is also accompanied by complications in the case of many data files. For instance, it does not deal well with partial blends and bands with complicated profiles – it might end the line prematurely. There is an even bigger problem which is caused by the fact that some lines in the spectrum may end very smoothly. While the program should have found the end of the line at some point, it will instead continue until it finds the point where the sign of the difference changes. These obstacles may be overcome by adding some conditions but improving this method to such a degree might be meaningless since there may be a better way of doing this.

The second approach to the determination of the outlining values of the line is to use the continuum. This can be done by starting from the centre of the line and checking all points that are below the continuum. Once the procedure finds a point above the continuum, it stops as it has found the end of the line. This is a better solution to the problem but is not without issues. For instance, if the line is partially blended, this procedure will result in integrating over at least part of the blended line as well. This inaccuracy gets even larger if the continuum is not found accurately enough – the procedure may not find the correct end of the line at all which will result in large errors in the calculation of the area. We have tried to account for these occurrences by putting in a condition that will stop the procedure at $0.98\,y_{\text{cont}}$. This results in the program finding the correct ends of the line but also introduces a small error due to the fact that it may sometimes skip many of the points of the line by ending too early or at the beginning. This error is insignificant in the case of very deep lines, but if the studied feature has the peak y-value at a small distance from the y_{cont} then the integration will not be done properly. We have used the fact that such interstellar lines are far too weak to be resolved properly and automatically set their equivalent widths to zero.

The program is written in Python and uses custom functions that are based on the procedures described above. The computation was done automatically – the program went through all of the 511 files containing data from X-Shooter spectrograph, took the wavelength and flux columns (not the reduced flux), and wrote the resulting equivalent widths to a separate file. Other data, like for example the declination and right ascension of the star, were can also be exported and used by transforming them to the Galactic coordinates for the purpose of creating maps. Finally, the functionality of the procedure was tested for the Na I lines at 5890 Å and 5896 Å (Figure 5.1) – the correlation between them is expected to be almost perfect.

5.4 Observing Known Interstellar Lines and DIBs

Several atomic interstellar lines can be observed in the X-Shooter spectra – they are listed in Table 5.1. Possibly most important are the lines of neutral sodium (5890 Å and 5896 Å) and ionized calcium (3934 Å and 3968 Å) which can be used for tracing diffuse phases of

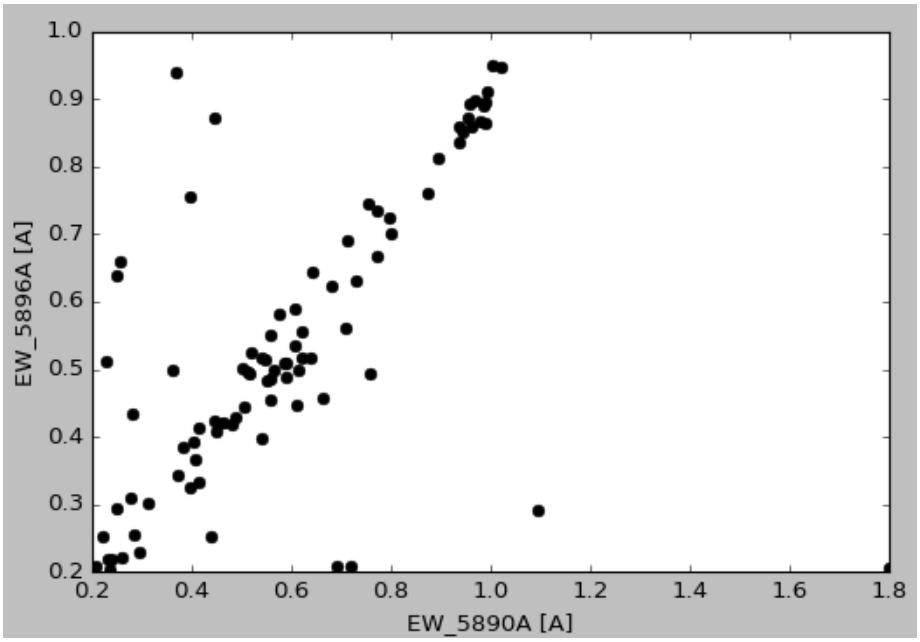

Figure 5.1: The correlation between the equivalent widths of the two Na I lines.

the ISM. On the other hand, spectral features of CH and CH^+ molecules can be used for studying denser parts of the medium. More molecules that would be interesting to compare with the strength of C_{60} lines are NH, CN, OH but their features could not be detected. Furthermore, when looking at models of atmospheres of cool stars and Sun, an absorption feature consisting of three peaks is present at 5780 Å, precisely at the location of one of the DIBs. With the use of an application called SpectroWeb, we have found that neutral Mn, Si, Fe and Ti have lines present at this wavelength. Of those, iron (3440.6 Å) and titanium (3383.7 Å, 3242.0 Å and 3229.2 Å) have interstellar lines present in the spectra used within this work – their relation to the DIB at 5780 Å should be searched for. According to the SpectroWeb, 6196 Å, 6271 Å, and 6614 Å bands are located near Fe lines as well.

Carrier	λ [Å]	Carrier	λ [Å]
Na I	3302	CH	3890
Na I	5890	CH	4300
Na I	5896	CH^+	3958
Ca II	3934	CH^+	4232.5
Ca II	3968	$^{13}CH^+$	4232.1
K I	7665	OH	3072
K I	7699	OH	3078
Ti II	3229	OH	3082
Ti II	3242	OH^+	3584
Ti II	3383	NH	3354
Fe I	3441	NH	3358
CH	3143	CN	3579
CH	3146	CN	3580
CH	3879	CN	3581

In the case of several stars, the profiles of calcium and sodium lines consisted of two components – a narrow interstellar part and a broadened part, possibly, of stellar origin (Figure 5.2).

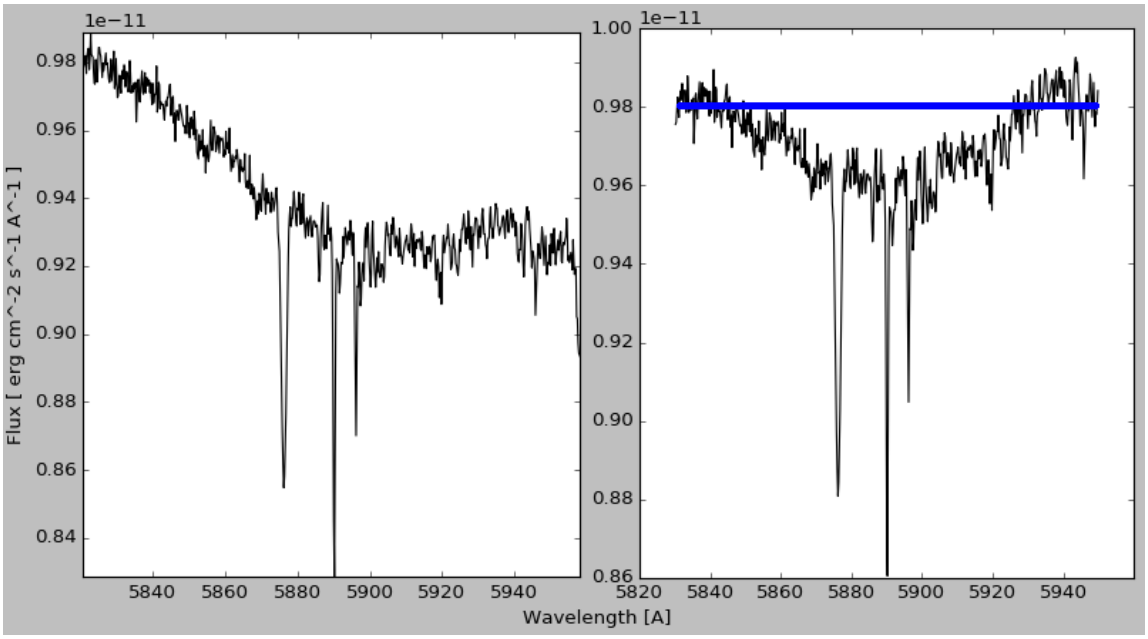

Figure 5.2: The broad feature seen towards HD 224926. The panel on the left shows the plot of the original data, the right panel displays the normalized spectrum with blue line being the estimated continuum in the area around the Na I spectral lines.

The very strong diffuse interstellar bands at 5780 Å, 5797 Å and 6614 Å can be easily resolved in many of the X-Shooter spectra. The broad 4430 Å feature, as well as weaker bands at 5850 Å, 6196 Å, 6270 Å, 6376 Å and 6379 Å are clearly resolved. However, the strong 6284 Å band is blended with a wide telluric band and 6376 Å and 6379 Å are sometimes blended together. We have chosen to measure equivalent widths of following six DIBs: 5780 Å, 5797 Å, 5850 Å, 6196 Å, 6271 Å and 6614 Å. Unfortunately, the bands at 9577 Å and 9632 Å are blended with telluric lines which are also present at these wavelengths. This makes the search for correlations with the C_{60} impossible and only those between the known carriers and the mentioned DIBs can be found without the removal of atmospheric features (Figure 5.3).

5.5 Presence of the Isotope Effect in Spectra

The theory predicts that if the C_{60} molecule is the carrier of the two DIBs then, as a result of the isotope effect, other bands should be present within several Å of these DIBs, with their strength depending on the isotope ratio of the place of origin of the molecule. Not much can be said about the isotope effect, since telluric features are present at the wavelengths of the two DIBs in the data used in this work. However, the possibility of observing this phenomenon can be, at least, estimated.

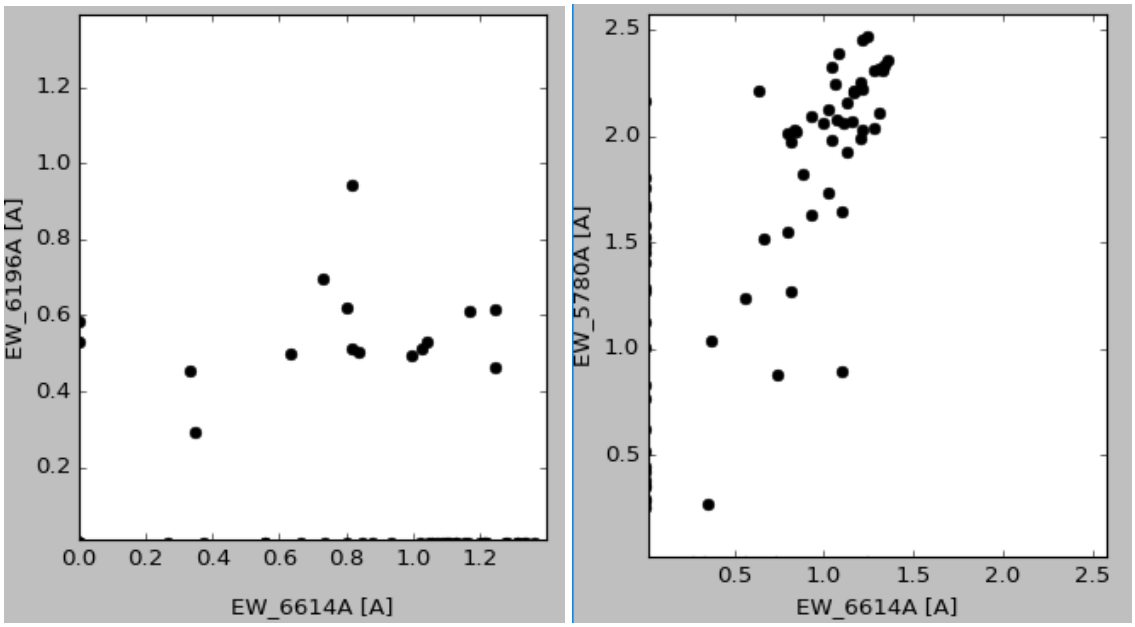

Figure 5.3: Correlations between the equivalent widths of the DIBs. In the left panel are the 6614 Å and the 6196 Å DIBs. In the right panel is the correlation between the 6614 Å and 5780 Å DIBs.

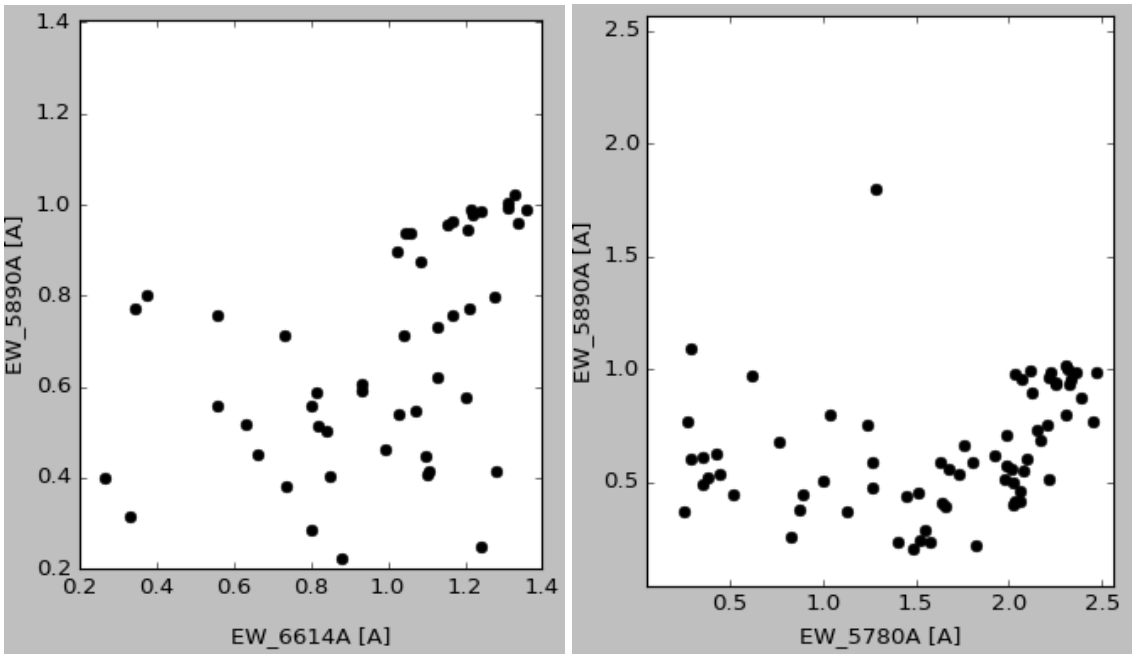

Figure 5.4: Correlations between the equivalent widths of two DIBs and the 5890 Å sodium line. In the left panel is the 6614 Å DIB and In the right panel is the 5780 Å DIB.

The full width at half maximum of the observed 9577 Å and 9632 Å bands is found to be between $2-3$ Å (see Foing & Ehrenfreund, 1997). This means that the band of another isotope should be located within the profile of the most abundant isotope of the molecule. In

order to distinguish between the two bands, observations with spectral resolution $R > 10\,000$ are required. This means that most of the data from the X-Shooter spectrograph might be used to determine the isotope structure of the two DIBs. If the structure is not found, an observation with a very-high-resolution spectrograph ($R > 100\,000$) would most likely give a definite answer on the question whether the C_{60} molecule is the carrier of these bands

Conclusions

In this thesis, we attempted to create a rovibrational model of the C_{60} molecule which is predicted (Campbell et al., 2015) to be the carrier of two of the diffuse interstellar bands at 9577 Å and 9632 Å. The model assumed that the molecule rotates as a rigid body and the vibrations were described by a Morse potential. The energy eigenvalues of such oscillator depend only on the oscillator frequency and on the dissociation energy. However, it is worth noting that such model would only work for radial oscillations and the C_{60} has only one such mode. The vibrational frequency of this mode is very low. Therefore, it is unlikely that vibrations alone could produce transitions at ~ 9000 Å region.

At first, we tried to use the advantage of having two known transitions. Since the oscillator frequencies have not been measured precisely enough to this date, we tried to find the frequency by testing several possible transitions that are likely to happen (vibrational states $n < 20$). This way, we were able to find the frequency $\nu \approx 932$ cm^{-1} which, in the given model, was able to produce transitions at both wavelengths. However, these transitions are very unlikely to happen ($\Delta n = 12$) even if such vibrational states are occupied. We were able to find observed spectral bands at other calculated wavelengths, but they could not be associated with these features since they represented telluric lines.

The second approach was relying on the knowledge of the vibrational frequency. From all of the experimentally observed frequencies, the $\nu = 1571.1$ cm$^-1$ was able to produce both of the DIBs with lowest transitions ($\Delta n = 7$) but did not precisely predict their wavelengths. One other DIB (13 175Å) also lied within the estimated range of another calculated line but, with the lack of any evidence, this assignment is very uncertain.

The next possibility is that the DIBs result from electronic transitions. In this case, electronic shift and oscillator frequency played the role of the unknown parameters and we searched for different combinations of their values. We were able to find such transitions that not only produce transitions at wavelengths of the DIBs but are also very likely to occur ($\Delta n = 1, 2$). The case of two different electronic shifts was studied, as well. The values of the shifts were taken from the literature and the vibrational mode was set as a known parameter ($\nu = 1419$ cm^{-1} produced best results). When looking at the first change of the vibrational quantum number, $1 \to 0$, we instantly got the transitions which can be matched with the DIBs. Furthermore, this is the only approach that provided positive results even at low temperatures (Campbell et al. worked with $T \sim 150$ K).

We also analysed the probability of finding the isotope effect of the C_{60} molecule in the spectra. There is a high probability of finding at least two different isotopes of this molecule because of the large number of carbon atoms it consists of. Sogoshi et al. (2000) found that the shift of the vibrational bands of the C_{60} can be significant ($\sim 0.5 - 2.0$ cm^{-1}). If the DIBs at 9577 Å and 9632 Å are originating from this molecule,

their isotope shifts should be observable. However, these shifts will be much smaller in the case of the electronic transitions and, therefore, much harder to detect.

Finally, we have written a simple procedure that can calculate the equivalent widths of the spectral lines. Before we could use it, we had to eliminate the telluric contamination from the X-Shooter data. Unfortunately, the procedure was not able to remove the telluric lines to the needed accuracy. This is due to the fact, that we used archival data which were not optimized to search for DIBs in this wavelength region. Therefore, we were only able to search for the correlations between the DIBs that are not caused by the C_{60} and several known interstellar lines. The 6196 Å and 6614 Å DIBs are usually very well correlated but we could not confirm this observational fact.

Bibliography

Bacchus-Montabonel, M.-C., & Wiesenfeld, L. 2013, Chem. Phys. Letters, 583, 23

Bakry, R., et al. 2007, International Journal of Nanomedicine, 2, 639

Berné, O., & Tielens, A. G. G. M. 2012, PNAS, 109, 401

Berné, O., Mulas, G., & Joblin, C. 2013, A&A, 550, 4

Brenner, D. W. 1990, PhysRevB, 42, 9458

Cami, J., et al. 2010, Science, 329, 1180

Campbell, E. K., et al. 2015, Nature, 523, 322

Cox, N. L. J., et al. 2014, A&A, 569, 117

Douglas, A. E., & Herzberg, G. 1941, ApJ, 94, 381

Draine, B. T., Physics of the Interstellar and Intergalactic Medium, Princeton University Press, Princeton and Oxford, 2011

Edwards, S. A., & Leach, S. 1993, A&A, 272, 533

Ehrenfreund, P., et al. 1992, A&A, 259, 257

Ferguson, A. M. N., et al. 1996, AJ, 111, 2265

Foing, B. H., & Ehrenfreund, P. 1997, A&A, 317, 59

Fulara, J., Jakobi, M., & Maier, J. P. 1993, Chem. Phys. Letters, 211, 227

García-Hernández, D. A., et al. 2010, ApJL, 724, 39

García-Hernández, D. A., et al. 2011, ApJL, 737, 30

Goto, M., et al. 2003, ApJ, 598, 1038

Haffner, L. M., Reynolds, R. J., & Tufte, S. L. 1999, ApJ, 523, 223

Heger, M. L. 1922, Lick Observatory Bulletin, 10, 148

Heiles, C., & Troland, T. H. 2003, ApJ, 586, 1067

Iglesias-Groth, S. 2004, ApJ, 608, 37

Inoue, T., & Inutsuka, S.-I. 2009, ApJ, 704, 161

Isobe, S., et al. 1986, Publ. Astron. Soc. Japan, 38, 511

Jing, D., & Pan, Z. 2009, Eur. J. Mech. A Solids, 28, 948

Jones, A., et al. 2013, A&A, 560, 91

Jäger, C., et al. 2009, ApJ, 696, 706

Kanekar, N., et al. 2003, MNRAS, 346, 57

Kaur, N., et al. 2007, arXiv:0704.2504

Kaźmierczak, M., et al. 2009, A&A, 498, 785

Kostant, B. 1994, PNAS, 91, 11714

Krełowski, J., et al. 1987, ApJ, 316, 449

Krełowski, J., et al. 1993, ApJ, 419, 692

Kroto, H. W., et al. 1985, Nature, 318, 162

Kroto, H. W., et al. 1987, ApJ, 314, 352

Kuntz, K. D., & Snowden, S. L. 2008, ApJ, 674, 209

Langer, W. D., & Penzias, A. A. 1990, ApJ, 357, 477

Langer, W. D., & Penzias, A. A. 1993, ApJ, 408, 539

Lobel, A., 2007, SpectroWeb: An Interactive Graphical Database of Digital Stellar Spectral Atlases, in ”The Ultraviolet Universe: Stars from Birth to Death”, 26th meeting of the IAU, Editorial Complutense Univ. of Madrid, ed. A. Gomez de Castro and M. Barstow, 167, Aug 2006, Prague, Czech Republic

Luna, R., et al. 2008, A&A, 480, 133

Léger, A., d'Hendecourt, L., & Défourneau, D. 1995, A&A, 293, 53

Marshall, C. C. M., Krełowski, J., & Sarre, P. J. 2015, MNRAS, 453, 3912

Matt, S., et al. 2001, Chem. Phys. Letters, 348, 194

Maíz-Apellániz, J. 2001, ApJ, 560, 83

McCall, B. J., et al. 2010, ApJ, 708, 1628

McKee, C. F., & Ostriker, J. P. 1977, ApJ, 218, 148

Menendez, J., & Page, J. B. 2000, in Light Scattering in Solids VIII: Fullerenes, Semiconductor Surfaces, Coherent Phonons, ed. M. Cardona, Güntherodt (Berlin: Springer), p. 27

Nandy, K., & Thompson, G. I. 1975, MNRAS, 173, 237

Noll, S., et al. 2012, A&A, 543, 92

Openov, L. A., & Podlivaev, A. I. 2006, JETP Lett., 84, 68

Otsuka, M., et al. 2014, MNRAS, 437, 2577

Palacios, A., et al. 2010, A&A, 516, 13

Parker, S. F., et al. 2011, Phys. Chem. Chem. Phys., 13, 7789

Pogulay, A. V., et al. 2004, Int. J. Mass Spectrometry, 233, 165

Reynolds, R. J. 1984, ApJ, 282, 191

Roy, N., Chengalur, J. N., & Srianand, R. 2006, MNRAS, 365, 1

Salama, F., et al. 2011, ApJ, 728, 154

Seon, K.-I. 2009, ApJ, 703, 1159

Signorell, R., & Kunzmann, M. K. 2003, Chem. Phys. Letters, 371, 260

Snow, T. P., York, D. G., & Welty, D. E. 1977, AJ, 82, 113

Sogoshi, N., et al. 2000, J. Phys. Chem., 104, 3733

Sonnentrucker, P., et al. 2010, A&A, 521, 12

Spitzer, L., Jr. 1956, ApJ, 124, 20

Tüllmann, R., et al. 2008, ApJ, 685, 919

Underwood, D. S., et al. 2016, MNRAS, 459, 3890

Vernet, J., et al. 2011, A&A, 536, 105

Verstraete, L. 2011, EAS Publications Series, 46, 415

Walker, G. A. H., Bohlender, D. A., & Krełowski, J. 2000, ApJ, 530, 362

Walker, G. A. H., et al. 2015, ApJ, 812, 8

Wdowiak, T. J. 1980, ApJ, 241, 55

Welsh, B. Y., et al. 2010, A&A, 510, 54

Weselak, T., et al. 2008, A&A, 484, 381

Witt, A. N., Bohlin, R. C., & Stecher, T. P. 1983, ApJ, 267, 47

Zhen, J., et al. 2014, ApJL, 797, 30

Zinner, E., et al. 2006, ApJ, 650, 350

Electronic Sources

Pollux Database:
http://npollux.lupm.univ-montp2.fr/DBPollux/PolluxAccesDB

SkyCalc Tool:
http://www.eso.org/observing/etc/skycalc/skycalc.htm

Spectroweb:
http://spectra.freeshell.org/spectroweb.html

X-Shooter Data Source:
http://archive.eso.org/wdb/wdb/adp/phase3_spectral/form